

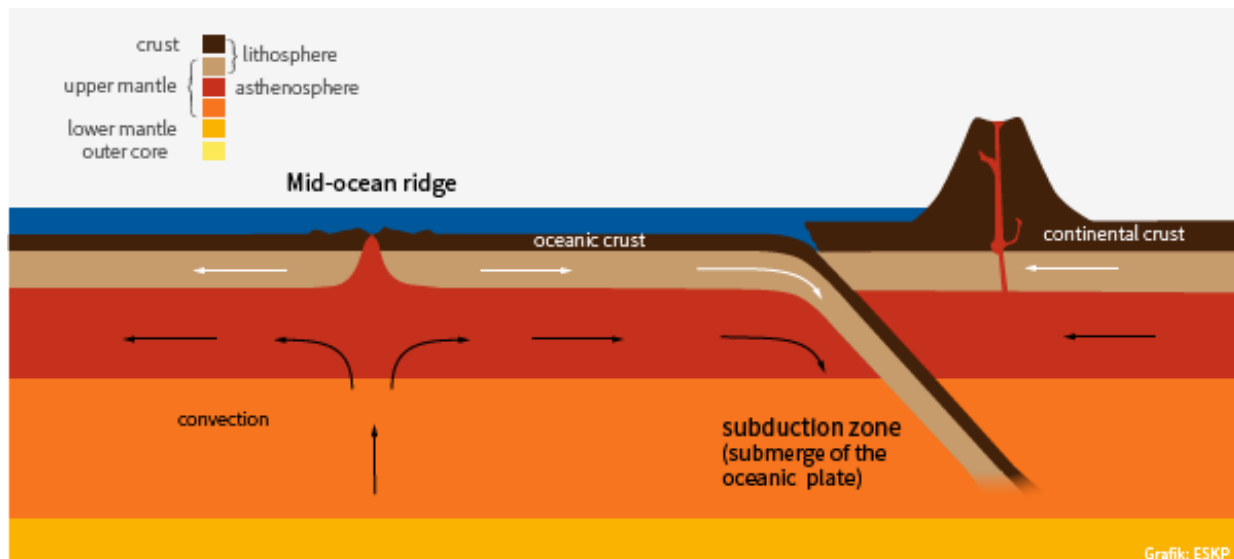
<p>Σχολή Θετικών Επιστήμων</p> <p>Τμήμα Γεωλογίας και Γεωπεριβάλλοντος</p> <p>Τομέας Ορυκτολογίας και Πετρολογίας</p> <p>Πανεπιστημιούπολη Ζωγράφου Αθήνα 15784 Ελλάς</p>	<p>National and Kapodistrian University of Athens</p>  <p>Εθνικόν και Καποδιστριακόν Πανεπιστήμιον Αθηνών</p>	<p>School of Sciences</p> <p>Faculty of Geology and Geoenvironment</p> <p>Department of Mineralogy and Petrology</p> <p>Panepistimioupoli Zographou Athens 15784 Greece</p>
---	--	---

Undergraduate Studies Program
Πρόγραμμα Προπτυχιακών Σπουδών
BSc Thesis – Προπτυχιακή Διπλωματική Εργασία

Temperatures of equilibration and oxygen fugacity conditions prevailing in the oceanic upper mantle at different tectonic settings

Συνθήκες θερμοκρασίας και πητικότητας οξυγόνου που επικρατούν στον ανώτερο ωκεάνιο μανδύα σε διάφορα γεωτεκτονικά περιβάλλοντα

Vasiliki Chatzitriantafyllou (Reg.No. 111420180128)
Βασιλική Χατζητριανταφύλλου (Α.Μ. 111420180128)



Athens, 2024
Αθήνα, 2024

Thesis Supervisor: Associate Professor Dr. Dimitrios Kostopoulos
Επιβλέπων: Αναπληρωτής Καθηγητής Δρ. Δημήτριος Κωστόπουλος
Acknowledgements

The present thesis was part of my BSc studies at the Faculty of Geology and Geoenvironment, National and Kapodistrian University of Athens, Greece. I would like to express my thanks to all those who contributed to the completion of this thesis and helped me achieve my goals. First of all, I would like to thank my supervisor, Professor of Metamorphic Petrology Dr. Dimitrios Kostopoulos, for the knowledge he provided me with, his valuable help and guidance, and for his contribution to developing my research skills and scientific thinking. I would also like to thank Professor Dr. Panagiotis Pomonis as well as the remainder of the Professors of the Department of Mineralogy and Petrology for their willingness to share their knowledge in their respective fields. Last, but not least, I would like to thank my family who never stopped believing in me and always supported me, as well as my friends who were always there for me.

Ευχαριστίες

Η παρούσα διπλωματική εργασία αποτέλεσε μέρος των πτυχιακών μου σπουδών στο Τμήμα Γεωλογίας και Γεωπεριβάλλοντος του Εθνικού και Καποδιστριακού Πανεπιστημίου Αθηνών. Θα ήθελα να ευχαριστήσω ορισμένα άτομα που συνέβαλαν στην ολοκλήρωση της παρούσας εργασίας και με βοήθησαν να πετύχω τους στόχους μου. Πρώτα απ' όλα, θα ήθελα να ευχαριστήσω τον επιβλέποντα καθηγητή μου, Δρ. Δημήτριο Κωστόπουλο, για τις γνώσεις που μου παρείχε, την πολύτιμη βοήθεια και καθοδήγησή του, καθώς και για τη συμβολή του στην ανάπτυξη των ερευνητικών μου δεξιοτήτων και της επιστημονικής μου σκέψης. Θα ήθελα επίσης να ευχαριστήσω τον καθηγητή Δρ. Παναγιώτη Πομώνη, καθώς και τους υπόλοιπους καθηγητές του Τμήματος Ορυκτολογίας και Πετρολογίας για την προθυμία τους να μοιραστούν τις γνώσεις τους στα αντικείμενά τους. Τέλος, θα ήθελα να ευχαριστήσω την οικογένειά μου που δεν έπαψε ποτέ να πιστεύει σε μένα και πάντα με στήριζε, καθώς και τους φίλους μου που ήταν πάντα δίπλα μου.

Abstract

This thesis presents a comprehensive study of the equilibration temperatures and oxygen fugacity conditions prevailing in the oceanic upper mantle across different tectonic settings, offering significant information on its chemical composition and dynamics. Through a detailed analysis of peridotites from mid-ocean ridges, metasomatized peridotites, and ophiolitic peridotites from supra-subduction zones, this study examines the impact of tectonic setting on various mantle processes. By calculating the temperatures of equilibration and oxygen fugacities of the samples, information was obtained regarding the thermal history and redox state of the upper mantle. The thesis reveals significant variations in temperature and oxygen fugacity, influenced by the tectonic environment, mantle source composition, partial melting, and fluid interaction. The results pinpoint the complex processes that occur in the oceanic upper mantle, contributing to its formation and evolution.

Σύνοψη

Η παρούσα πτυχιακή εργασία παρουσιάζει μια ολοκληρωμένη μελέτη των θερμοκρασιών ισορροπίας και των οξειδωτικών συνθηκών που επικρατούν στον ανώτερο μανδύα σε διάφορα γεωτεκτονικά περιβάλλοντα, προσφέροντας σημαντικές πληροφορίες για την χημική του σύσταση και τις διεργασίες που λαμβάνουν χώρα εκεί. Μέσω μιας λεπτομερούς ανάλυσης περιδοτιτών από μέσο-ωκεάνιες ράχες, μετασωματωμένων περιδοτιτών, και οφιολιθικών περιδοτιτών υπέρθεν ζωνών υπαγωγής, εξετάζεται η επιρροή των τεκτονικών περιβαλλόντων σε διάφορες διεργασίες του μανδύα. Μέσω του υπολογισμού των θερμοκρασιών ισορροπίας και της πτητικότητας του οξυγόνου, αποκτήθηκαν πληροφορίες σχετικά με την θερμική ιστορία και την οξειδοαναγωγική κατάσταση του ανώτερου μανδύα. Η έρευνα αυτή αποκαλύπτει σημαντικές μεταβολές στην θερμοκρασία και στην πτητικότητα του οξυγόνου, υπό την επιρροή του τεκτονικού περιβάλλοντος, της σύστασης της μανδυακής πηγής, της μερικής τήξης και της αλληλεπίδρασης με ρευστά. Τα αποτελέσματα καταδεικνύουν τις πολύπλοκες διεργασίες που λαμβάνουν χώρα στον ωκεάνιο μανδύα, και συμβάλλουν στον σχηματισμό και την εξέλιξη του.

Table of Contents

1. Introduction	5
1.1 The oceanic upper mantle	5
1.2. Mid-Ocean Ridges	6
1.3 Supra-Subduction zones	7
1.4 Forearcs.....	10
1.5 Back-arcs	11
2. Mineralogy	13
2.1 The depleted mantle.....	13
2.2 Mantle peridotite mineralogy.....	14
2.2.1 Non-metasomatized abyssal peridotites	14
2.2.2 Metasomatized abyssal peridotites	14
2.2.3 Supra-subduction zone peridotites.....	15
2.3 Spinel composition in the Cr-Al-(Fe ³⁺ +2Ti) space.....	16
2.4 Peridotite characterization by olivine–spinel compositional relationship	19
2.5. Spinel Al ₂ O ₃ - TiO ₂ systematics.....	21
2.6 Spinel Ti - Cr# systematics.....	23
3. Thermometry and Oxybarometry	26
3.1. Introduction to geothermometry	26
3.2 Olivine-Spinel thermometry – Thermodynamic background	26
3.3 Olivine-Spinel thermometry - Applications.....	27
3.3.1 The BBG91 geothermometer.....	27
3.3.2 The LKVF95 geothermometer	28
3.3.3 Comparison between the BBG91 and LKVF95 geothermometers.....	30
3.4 Oxybarometry and the redox state of the upper mantle	32
3.5 Redox state of spinel peridotites according to their Cr# in correlation with temperature	33
3.6 Redox state of peridotites in correlation with the Fe ³⁺ /ΣFe ratio of spinels	39
4. Summary and conclusions.....	42
4.1 Results from peridotite spinel chemistry.....	42
4.2 Results from olivine-spinel equilibration temperatures and oxygen fugacities	43
References	45

1. Introduction

1.1 The oceanic upper mantle

The oceanic upper mantle is an important component of the Earth's geology and plays an important role in various geological processes and the formation of the oceanic lithosphere. It extends from the bottom of the crust to a depth of about 660 km, encompassing a complex and dynamic environment. Understanding the petrology of the Earth's oceanic upper mantle can provide important insights into the composition, structure, and geodynamic processes that shape the planet. In this introduction, I will focus on the Earth's upper oceanic mantle's main features and petrological properties, emphasizing its geological importance.

The oceanic upper mantle mainly comprises ultramafic rocks rich in ferromagnesian minerals such as olivine, spinel, pyroxene, and garnet. These rocks are formed by partial melting of the mantle below mid-ocean ridges, where upwelling mantle material undergoes decompression melting at shallower depths due to reduced pressure. The resulting magma rises to the surface, forming a new oceanic crust. As the molten rock cools and solidifies, it forms a layered sequence of igneous rocks known as the oceanic lithosphere.

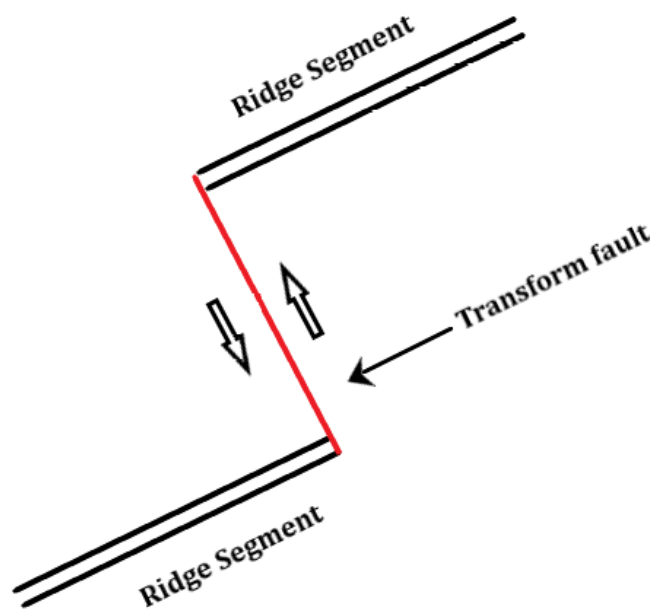
The composition of the upper mantle depends on the different tectonic settings. According to many researchers, the chemistry and mineralogy of peridotite differ among alternative locations and sites. Olivine and spinel are dominantly magnesian and are useful indicators of mantle processes. The presence of pyroxene minerals such as orthopyroxene and clinopyroxene provides further information about the temperature and pressure conditions prevailing in the mantle. In addition, peridotite chemistry can highlight the mode of formation of the oceanic crust through partial melting. Peridotite mineral chemistry reflects the thermodynamic state of the upper mantle in different tectonic settings and any shift in these conditions is faithfully recorded by the minerals. On the other hand, peridotite whole-rock composition is controlled by partial melting and metasomatism processes mainly displaying compositional depletion with the melt extracted concentrating at mid-ocean ridges and forming the bulk of the oceanic crust.

Furthermore, the oceanic upper mantle is not a homogeneous region. It exhibits significant heterogeneity due to several factors, including the recycling of oceanic crust at subduction zones (Pacific Ocean, etc.) and the formation of mantle plumes (Hawaii hotspot, etc.). These processes lead to the addition of different components and the formation of different mantle regions with different chemical and mineralogical compositions.

In recent years, advances in analytical techniques such as electron microscopy, X-ray spectroscopy, and isotope analysis have greatly elevated our understanding of the petrology of the Earth's oceanic upper mantle. These techniques allow researchers to study the mineralogy and chemical changes that take place in mantle rocks and gain valuable insights into processes happening deep inside the Earth.

1.2. Mid-Ocean Ridges

Mid-ocean ridges (MORs) are undersea mountains with rifts in their middle. A MOR corresponds to the divergent edge of two plates, where the crust is expanding and forming a new seabed, which is moving away from the ridge at a rate of 2 to 10 centimeters per year. The material under a MOR rises as the pressure decreases, thereby undergoing partial melting. The produced magma is collected in magma chambers several kilometers below the seafloor and most of it eventually freezes in place, forming most of the new oceanic crust.



Picture 1: Illustration of a transform fault.

Mid-ocean ridges represent the largest and most dynamic geological features on Earth, expanding thousands of kilometers across the ocean floor. The interplay of tectonic and magmatic processes shapes the complex structures and features along mid-ocean ridges. Volcanic activity is a prominent feature of these environments, with magma erupting from the mantle through fractures and cracks, forming volcanic cones, lava flows, and pillows. Understanding the dynamics of magma supply, eruption frequency, and lava composition is critical to understanding the evolution of mid-ocean ridges. In addition, tectonic processes such as faulting, rifting, and transform faulting contribute to the growth and segmentation of ridge systems and influence the overall morphology

and tectonic activity of these oceanic rift zones. Transform faults are very important in accommodating the lateral movement of plates; as the plate diverges along the ridge, the transform faults intersect the ridge axis at right angles, forming offset segments (Picture 1). These faults allow the crustal blocks to move horizontally, effectively transmitting the stress and strain generated by the divergent motion. Transform faults act as a safety valve, preventing excessive stress along the ridge and allowing smooth, continuous movement of the plates. Without transform faults, pressure can build up along the ridge, potentially leading to a catastrophic seismic event. Therefore, these faults play a crucial role in maintaining the dynamic balance between the mid-ocean ridge system and the involved plate tectonics.

The petrology of a MOR varies, depending on factors such as the spreading rate of the ridge, the location of the ridge, and the chemical composition of the mantle beneath the ridge. Abyssal peridotites are the result of mantle upwelling when new oceanic lithosphere is formed. They mainly consist of four lithology types (Warren, 2016). The first and more common type is residual peridotites. Residual peridotites are the result of partial melting. When the mantle beneath the mid-ocean ridges undergoes melting, some of the molten rock rises to form a new oceanic crust, while the remaining residue of the mantle remains solid and forms the residual peridotites. These rocks can provide valuable information about the composition and history of the mantle, as well as the processes involved in the formation of new oceanic crust. The second representative petrological group is dunites. Dunites are composed primarily of the mineral olivine (>90% olivine), with low contents of pyroxene and chromite. They are evaluated as porous flow channels that transfer the majority of melt out of the mantle. A large percentage of them is also found to be altered due to serpentinization of the olivine, as it's their major component. Another representative lithology found in most MORs is gabbro-veined and/or plagioclase-bearing peridotites. These peridotites contain plagioclase-bearing minerals and/or veins of gabbro. The presence of gabbro in the peridotite indicates partial melting, causing gabbro to crystallize in veins inside the peridotite. On the other hand, plagioclase-bearing minerals inside the peridotites indicate metasomatic processes (contact with surrounding rocks or metasomatic fluids) that have changed their chemical consistency. The fourth lithology that represents abyssal peridotites is pyroxenite-veined peridotites. This group is the outcome of recycling old oceanic crust, or of recent melt crystallization and metasomatism. Pyroxenes found in these peridotites are either coming from parts of the old ocean lithosphere and are high in silica or from metasomatic events and vary in chemical composition (secondary pyroxenites).

Hydrothermal activities are also a phenomenon that plays a crucial role in the geological processes that take place in a MOR environment. Hydrothermal fluids, seawater that makes its way inside the oceanic lithosphere through cracks, reaches high temperatures, and gets enriched with elements. These fluids, react with the rocks in contact, altering their chemistry and metasomatizing them. These fluids emanate from the oceanic crust in the form of hydrothermal vents such as black or white smokers.

1.3 Supra-Subduction zones

A supra-subduction zone setting refers to a geological environment where an oceanic plate is being subducted beneath another plate, composing various geological and tectonic features. These zones are scientifically interesting as they play a vital role in the Earth's geodynamic processes, the formation of continental crust, and mountain formation.

The formation of supra-subduction zones involves a chain of tectonic processes. They primarily occur at convergent plate boundaries, where two plates are moving toward each other. The process starts when an oceanic plate collides with another oceanic or continental plate. The denser oceanic plate is forced beneath the less dense continental or oceanic plate, leading to subduction. The heavier oceanic plate undergoes intense pressure and heating as it sinks into the mantle. At certain depths, the subducting plate starts to release water and carbon dioxide trapped in the minerals of the oceanic crust. These fluids cause partial melting of the mantle wedge that lies above the plate, leading to the formation of magma.

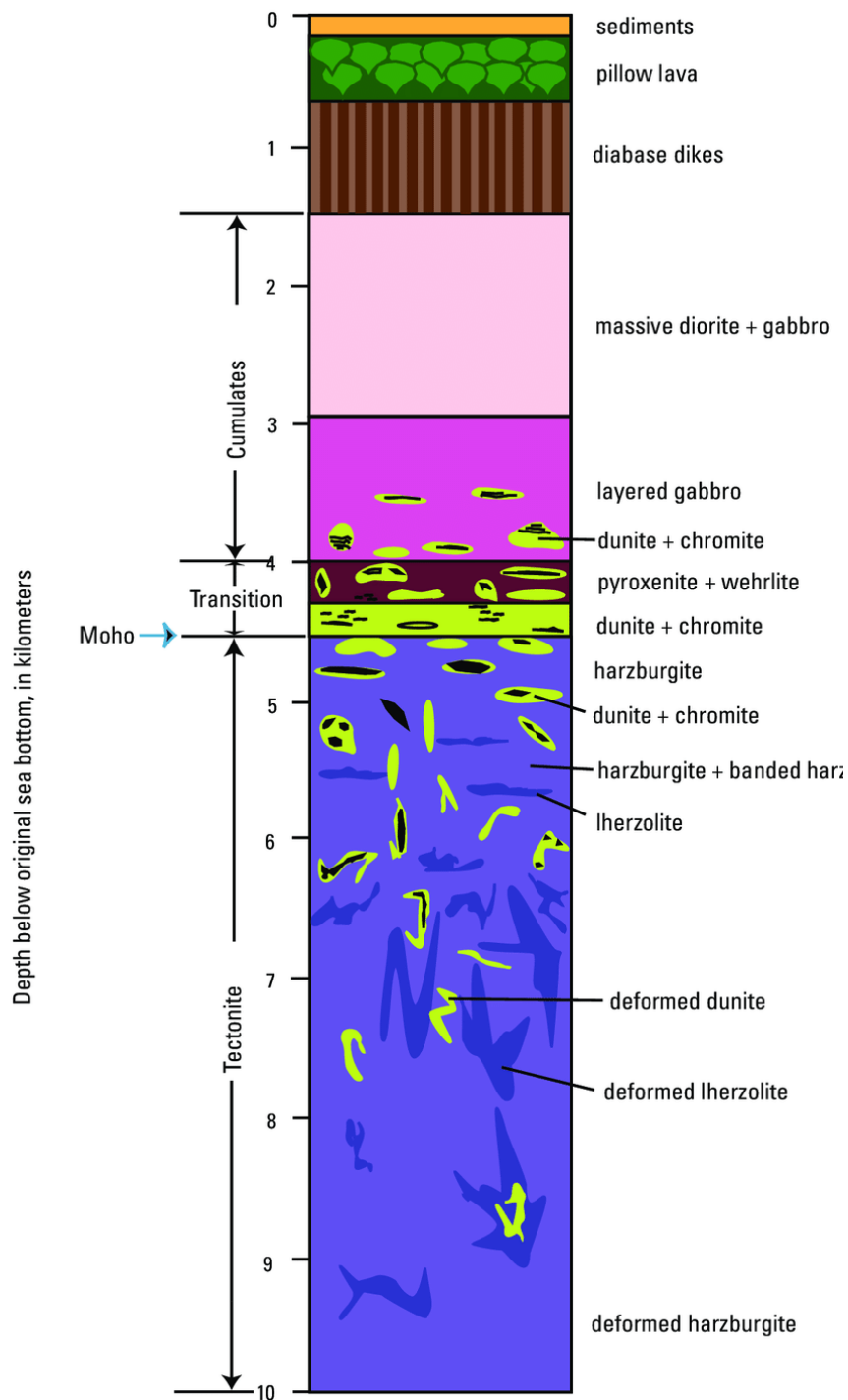
One of the most pointed features of a supra-subduction zone is the formation of the subduction trench which represents the surface expression of the subduction process. Another distinctive part of an SSZ is volcanic arcs. As the magma, produced in the mantle wedge rises toward the surface, it leads to the formation of volcanoes along the overriding plate. These volcanoes form an arc parallel to the trench, which marks the location of subduction. These volcanic arcs are often associated with explosive and effusive eruptions, as they participate in the expansion of the crust.

Other characteristic formations that are part of an SSZ are forearc basins that are located between the volcanic arc and the subduction trench and back-arc basins that are formed behind the volcanic arc, between the volcanic arc and the continental margin.

Concerning the petrological finds in such settings, SSZ ophiolites are the most representative example and the petrological group of this setting that we are going to examine petrologically in this thesis. Ophiolite complexes are characterized by a sequence of groups of ultramafic and mafic rocks. In a complete ophiolite sequence, there are four sets of igneous rocks from top to bottom (Picture 2):

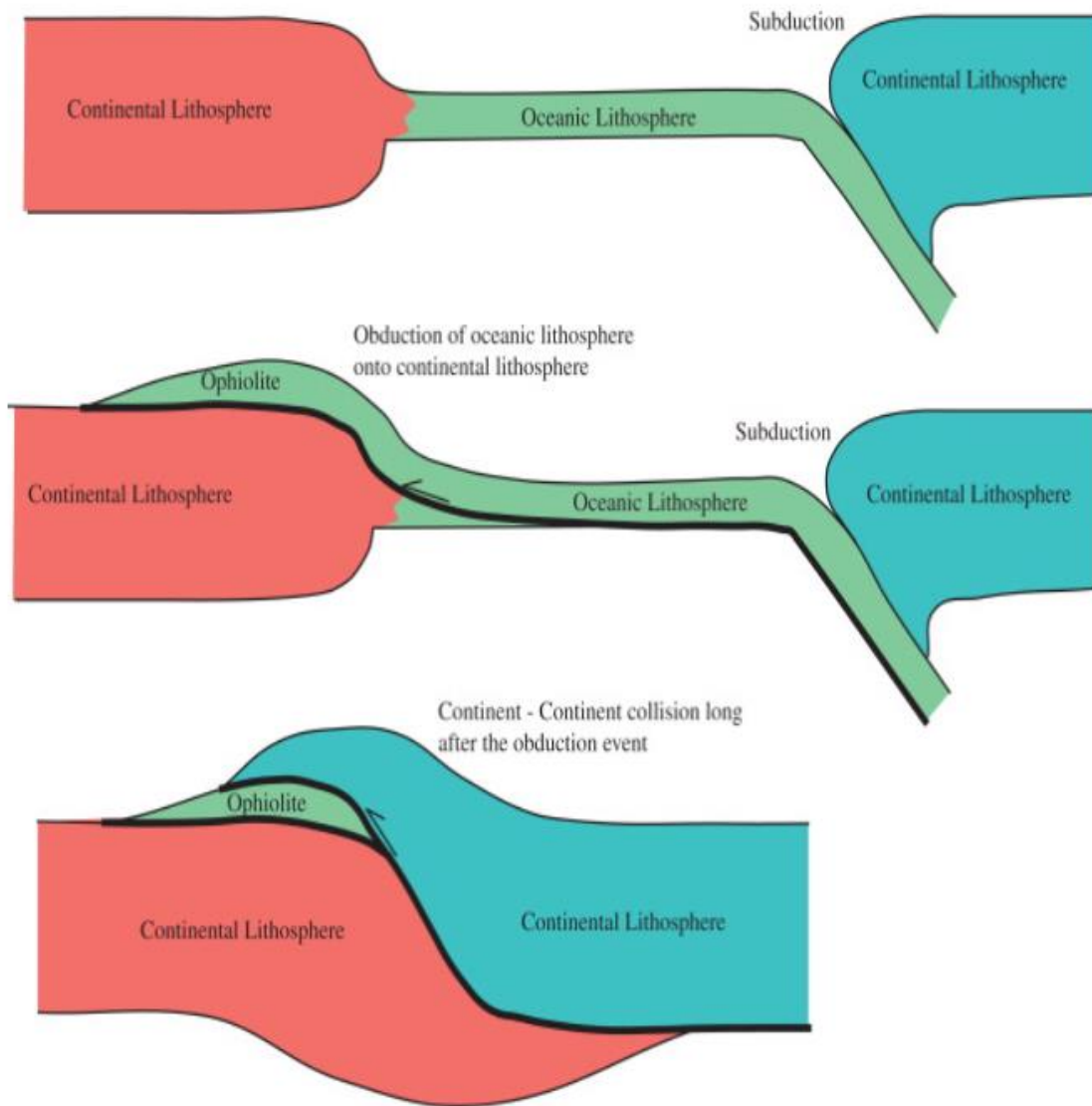
1. Pillow lavas: Basalt lavas form pillows at the top of the ophiolite complex.
2. Sheeted dykes of micro gabbro
3. Cumulate rocks: The result of fractional crystallization of basaltic magma.
4. Tectonites: They are mechanically overstressed, mantle ultramafic rocks.

Supra-subduction zone (SSZ) ophiolites have the geochemical characteristics of island arcs but the structure of the oceanic crust and are thought to have formed by seafloor spreading directly above subducted oceanic lithosphere (Pearce, 2016). SSZ ophiolites represent segments of SSZ oceanic lithosphere that have been thrust onto the continental crust during tectonic collisions (Picture 3).



Picture 2: Ideal stratigraphic section of an ophiolite complex. (https://www.researchgate.net/figure/Generalized-stratigraphic-column-of-an-ophiolite-sequence-showing-the-zones-with-their_fig3_233947458)

Regarding the petrology of SSZ ophiolites, their geochemical and mineralogical compositions reflect the geological processes that take place in supra-subduction environments. SSZ ophiolites consist of forearc basalts, boninites and island-arc tholeiites, which indicate a subduction history.



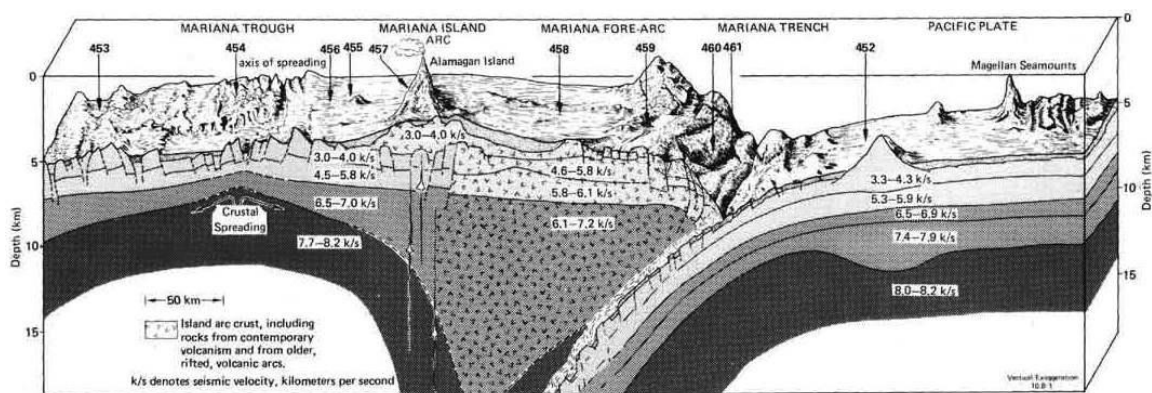
Picture 3: A schematic cross-section that shows ophiolite obduction onto a continental margin followed later by continent-continent collision (<https://www.sciencedirect.com/topics/earth-and-planetary-sciences/ophiolite>).

1.4 Forearcs

A forearc begins to form at an SSZ setup, as an oceanic plate subducts beneath another oceanic plate or a continental plate. The descending plate forms the subduction slab, which begins to sink into the Earth's mantle. As the oceanic plate subducts, it carries along sediments from the ocean floor. These materials accumulate in the trench and can undergo metamorphism due to the T-P conditions prevailing deep down in the trench. While the oceanic plate keeps sinking into the mantle, it begins to heat up and dehydrate. The hydrous fluids thus released flush the overlying mantle wedge that undergoes partial melting. The molten material, rises through the overlying mantle and crust, forming

eventually a volcanic arc in the surface. Between the trench and the volcanic arc, forms a depression, which is defined as the forearc basin. This basin is usually filled with sediments eroded from the surrounding area, including the volcanic arc. The ongoing process of subduction in combination with the tectonic activity leads to the final formation of the forearc. Some of the most representative forearc environments are the Mariana forearc and the Izu-Bonin forearc which are found in the Western Pacific Ocean.

The Mariana Forearc which is one of the most known forearc basins, is located between the Mariana Trench and the Mariana Islands covering a space of 200 km wide and 1500 km long. According to samples gathered from drilling at the Mariana forearc basin, the dominant petrological types are harzburgites and dunites with most of them being strongly serpentinized (Yasuhiko Ohara, 1998).



Picture 4: The Mariana Subduction Zone.

In general, the petrology of forearc peridotites can vary based on factors such as the thermal regime, pressure-temperature conditions, the extent of mantle melting, and the presence of fluids associated with subduction. The presence of certain minerals like olivine and spinel can be influenced by the depth and pressure at which the peridotites formed. The majority of forearc peridotites are harzburgites with higher spinel #Cr and olivine Fo content, in comparison with abyssal peridotites (Arai, 1994).

1.5 Back-arcs

Back-arc environments are tectonic settings associated with subduction zones. Back-arc basins are typically formed at convergent plate boundaries where one plate is being forced beneath another. This type of boundary is known as a subduction zone. One of the plates is usually an oceanic plate or a continental, whereas the plate that is denser and moves underneath is oceanic. As the oceanic plate is pulled downward into the Earth's mantle at the subduction zone, it starts to dehydrate due to the increasing temperature and pressure. This process causes melting of the overlying mantle wedge and the magma produced moves upward to the surface. The rising magma pierces through the overriding

plate and forms a volcanic arc. The volcanic arc is parallel to the oceanic trench, located at some distance from it. As the oceanic plate continues to subduct, the overriding plate behind the volcanic arc begins to accept extensional forces. The subduction of the oceanic plate creates a tensile force, causing the lithosphere of the overriding plate to stretch and thin and lead to the formation of a basin behind the volcanic arc. This basin is called the back-arc basin. As the lithosphere stretches and thins, it allows space for the basin to sink, and it is often filled with sediment from the surrounding regions. While the thinning of the lithosphere continues, it leads to the formation of new oceanic crust. Most back-arc peridotites, seem to be lherzolites and clinopyroxene-bearing harzburgites high in Fo content (Arai, 1991).

2. Mineralogy

2.1 The depleted mantle

The depleted MORB mantle (DMM) is a part of the upper mantle that has experienced significant depletion in certain elements (mostly incompatible trace elements, i.e. elements that do not fit into the crystal lattices of mantle minerals) and isotopes. The DMM serves as the source reservoir to mid-ocean ridge basalts (MORBs), and represents 30% of the mass of the whole silicate Earth. Compared to the primitive mantle (PM), DMM has only 15% of its radiogenic heat production. (Workman, Hart, 2005).

Modal Abundances in DMM (%):							
	Olivine	Opx	Cpx	Spinel			
	57	28	13	2			
Mineral compositions:							
	Olivine	Opx	Cpx	Spinel	Bulk DMM	PUM ^a	Primary N-MORB ^b
SiO ₂	40.70	53.36	50.61		44.71	44.90	49.51
Al ₂ O ₃		6.46	7.87	57.54	3.98	4.44	16.75
FeO ^c	10.16	6.27	2.94	12.56	8.18	8.03	8.05
MnO	0.14	0.12	0.09	0.16	0.13	0.13	0.14
MgO	48.59	30.55	16.19	19.27	38.73	37.71	9.74
CaO	0.05	2.18	19.52		3.17	3.54	12.50
Na ₂ O		0.05	0.89		0.13 (0.28) ^d	0.36	2.18
Cr ₂ O ₃		0.76	1.20	10.23	0.57	0.38	0.07
TiO ₂		0.16	0.63		0.13	0.20	0.90
NiO	0.36	0.09	0.06	0.24	0.24	0.25	–
K ₂ O					0.006 ^e	0.029	0.065
P ₂ O ₅					0.019 ^f	0.021	0.095
Total	100.00	100.00	100.00	100.00	100.00	100.00	100.00

Table 1: Table of Modal Abundances and major elements composition of the Depleted MORB mantle, the Primitive upper mantle, and the Primary MORB mantle (Workman-Hart, 2005).

Workman and Hart (2005) examined the composition of the average DMM as shown above in Table 1. These results were retrieved from the examination of abyssal peridotite samples based on a global scale, indicating depletion of the primitive mantle by 2-3% melt extraction. The isotopic composition of rocks derived from the DMM shows distinct patterns compared to the primitive mantle revealing information about differentiation and mixing with other mantle sources.

On the other hand, the primitive mantle qualifies for the initial composition of the Earth's silicate portion, representing the (lower) part of the mantle that has experienced no melting. MORBs dredged from hot spots are great indicators of the PM's chemical composition with higher contents of incompatible elements such as K, Rb, Cs, Ba, and

LREE. Also, higher concentrations of SiO₂, Al₂O₃, Na₂O, and CaO and lower concentrations of MgO are leading to chemical compositions of PM-derived rocks.

In conclusion, the DMM is the outcome of the PM's partial melting (by 2-3%), with an average modal composition: $Ol_{57}Opx_{28}Cpx_{13}Spl_2$. Average DMM constrains parental MORB to be generated by 6% aggregated fractional melting.

2.2 Mantle peridotite mineralogy

2.2.1 Non-metasomatized abyssal peridotites

Abyssal peridotites have been most frequently sampled from oceanic fracture zones, where their emplacement is one of the great enigmas of marine geology (Dick, 1989). Situated near the top (base of the crust), they display the top section of the mantle, that has been brought up due to pressure release melting of the mantle under mid-ocean ridges. For this thesis, data were used from samples of abyssal peridotites from Warren (2016), and their geochemical properties were reviewed according to their composition. The samples that were used are 900 and cover a wide range of localities. The ridge segments that they cover are the **East Pacific Rise, Southwest Indian Ridge, Mid-Atlantic Ridge, America-Antarctic Ridge, Central Indian Ridge, Gakkel Ridge**, and the **Lena Trough** with EPR spreading the fastest and GAK having the slowest spreading rate accompanied by SWIR and AAR. Slow-spreading mid-ocean ridges typically have a smaller magma supply and lower mantle upwelling rates compared to fast-spreading ridges. This results in a more prolonged period of partial melting in the mantle beneath the ridge. Therefore, abyssal peridotites from slow-spreading ridges are more likely to have experienced extensive partial melting. About the petrography and composition of the samples, the majority are harzburgites and gabbro-veined peridotites with a significant percentage of dunites. There is also a dataset of metasomatized peridotites given by Warren (2016), which is going to be reviewed next.

2.2.2 Metasomatized abyssal peridotites

Metasomatized peridotites are peridotites that have undergone metasomatism and the chemical composition of the rock is changed through the exchange of chemical elements and compounds with fluids and melts. Metasomatism can occur due to various geological processes and can provide insight into the processes that take place in the Earth's mantle and the chemical interactions between the mantle and various melts and fluids. For this thesis, data of metasomatized abyssal peridotites from Warren (2016) were used to

examine their geochemistry according to their composition. There are 175 samples of metasomatized peridotites and they consist of dunites containing either gabbro or pyroxenite veins, gabbro-veined and/or plagioclase-bearing peridotites, pyroxenite-veined peridotites, and a small dataset of harzburgites that even though they do not contain veins of other minerals, they showcase melt inclusions, higher Ti contents and LREE enrichments.

2.2.3 Supra-subduction zone peridotites

Ophiolites is the type of oceanic lithosphere that is usually associated with subduction zones. They are fragments of ancient oceanic crust and upper mantle that were tectonically emplaced through different mechanisms onto the surface of the Earth. For this thesis, 400 samples of ophiolites from various locations were used. The first and most important site that was examined petrologically is the **Yarlung-Tsangpo** suture zone. The Yarlung-Tsangpo suture zone is a major geological structure associated with the closure of the Tethys Sea and the collision between the Indian and the Eurasian plates (Wang et al., 2000) and contains the Himalayan ophiolites. The Yarlung-Tsangpo suture zone formed where the Indian plate collided with the southern margin of the Eurasian plate. The ophiolites assemble the remnant of the Tethys Ocean floor along with continental fragments, that have been accumulated to the southern margin of Eurasia. Current models suggest that most of the East Tethyan lithosphere was subducted within a single subduction zone, active during the mid Cretaceous (Coulon et al., 1986) and closed during continental collision (Rowley, 1998). Ophiolite complexes from Yarlung-Tsangpo suture zone that are included in this thesis are the Purang, Kangjinla, Luobusa, Dongbo, Dazhuqu, and Cuobuza complexes. The second location that was examined is **Oman**. The Oman ophiolites are fragments of the Tethyan oceanic lithosphere formed at the fast-spreading center that was emplaced onto the Arabian continent (Lippard et al., 1986). It is suggested that their formation occurred from a second-stage (arc-type) magmatism above a subduction zone (Akizawa et al., 2012). The next complex that was examined is the **New Caledonian** ophiolite, located in the southwestern Pacific Ocean. New Caledonia consists of four major tectonic units: the pre-Cretaceous basement terranes, the HP-LT metamorphic belt, the Poya terrane (basalts), and the peridotite Nappe (Cluzel et al., 2001). Another complex that has been examined in this thesis is the **Yushigou** ophiolite. The Yushigou ophiolite is located in the North Qilian suture zone at the northern margin of the Tibetan Plateau and is part of the Qinling-Qilian-Kunlun fold system of NW China. The Yushigou ophiolite is the oldest complex in the North Qilian belt with U-Pb zircon crystallization ages of gabbro and pillow basalt of 530-560 Ma (Shi et al., 2004; Song et al., 2003). An additional complex that was examined is the **Miyamori** ophiolitic complex, Japan. The Miyamori ophiolitic complex is a thrust sheet emplaced along the Hayachine tectonic belt (Ozawa, 1988). Later tectonic events led to the transportation of the complex southward along the Hizume-Kesennuma sinistral

transcurrent fault (Ozawa, 1984). This movement was the cause of the breakage of the continuous complex in the Hayachine tectonic belt, into two different complexes with similar petrographic characteristics and geochemical properties, the Miyamori and Hayachine complexes. The next ophiolitic complex that was examined is the **Zambales** ophiolitic complex, located on the island of Luzon, Philippines. This complex includes the Coto and Acoje blocks and forms part of the basement of the Luzon island arc complex. Southwest Turkey ophiolites were also examined in this thesis; they have been interpreted as a series of remnants of one of several possible southern branches of Neotethys—the **SW. Turkey** ophiolites were emplaced along the margin of the Bey Daglari carbonate platform. The last ophiolitic complex that was examined in this thesis is the **SW. Oregon** ophiolite, located in the Coast Ranges Province of Southwestern Oregon. These specific rocks had a complex history including the derivation from oceanic mantle and tectonic emplacement on the Coast Ranges Province during Cretaceous times. In addition, they were modified by Late Cenozoic vertical faults and protrusions associated with recent diapiric movements (Henry & Medaris, 1980).

2.3 Spinel composition in the Cr-Al-(Fe³⁺+2Ti) space

Peridotite spinels from the world's mid-ocean ridges and ophiolitic complexes discussed above have been plotted on the Cr-Al-(Fe³⁺+2Ti) ternary diagram to specify their type (Figures 1-4). As Figures 1 and 2 show, most spinels from non-metasomatized abyssal peridotites are classified as aluminum chromites with a subordinate population classifying as chromian spinel. It is noticeable that the samples with high-Cr spinel come from the EPR whereas some come from the MAR as well. The higher Cr content in these samples is associated with a more depleted mantle source and a higher degree of melting. The samples with higher Al indicate smaller degrees of partial melting. EPR is the fastest spreading among all ridges producing more melt than other ridges thus displaying the most Cr-rich spinel compositions. Regarding metasomatized abyssal peridotites, most spinels are classified as aluminum chromites with a smaller population plotting in the field of chromian spinel (Fig. 3). The samples with higher Cr contents (mostly from MAR and EPR) indicate that they were derived from a more depleted mantle, in comparison with samples high in Al (mostly from SWIR), which indicate a more fertile mantle source. Interestingly, some samples display a trend toward higher Fe³⁺+2Ti pointing to the fact that these samples have been influenced by metasomatic melts. Contrary to spinels from abyssal peridotites, most spinels from SSZ ophiolitic peridotites are chromian spinels with Cr# [Cr/(Cr+Al)] ranging from 0.5-0.9, indicating a very depleted source. All samples from New Caledonia have Cr#>0.5, whereas those from Oman tend to be higher in Fe³⁺+2Ti indicating melt infiltration and/or metasomatic activity.

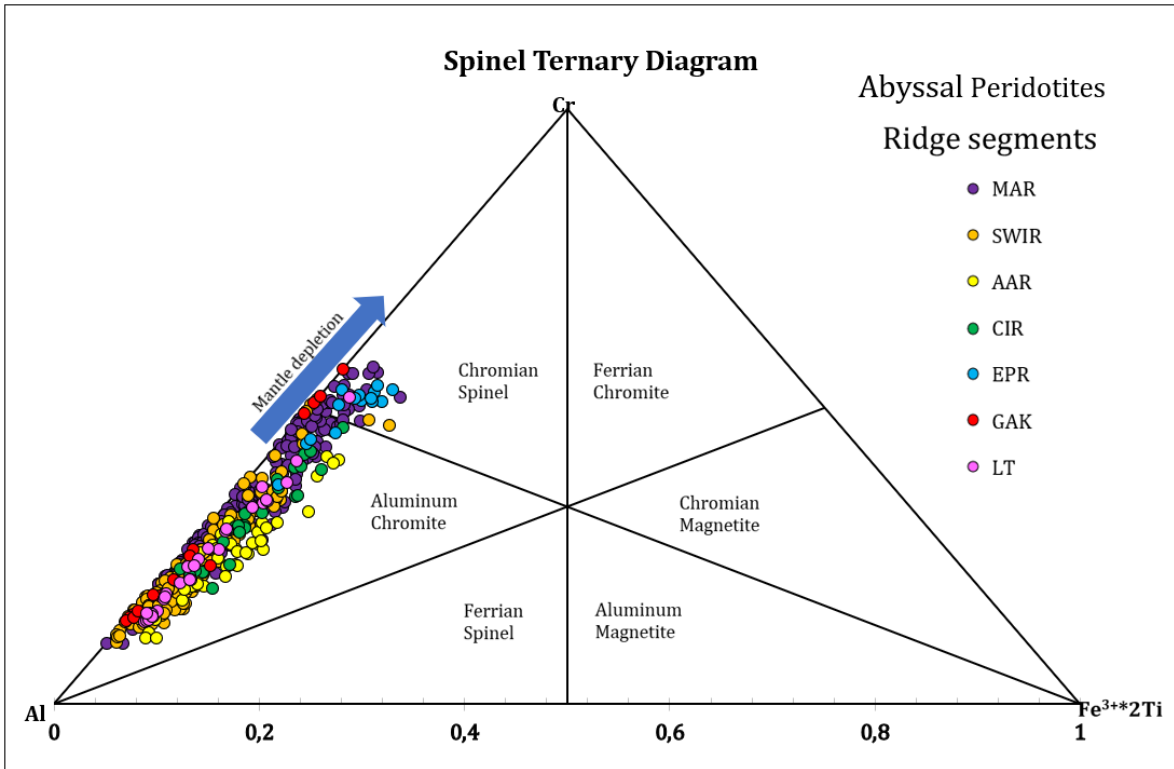


Figure 1: Spinel types in non-metasomatized abyssal peridotites.

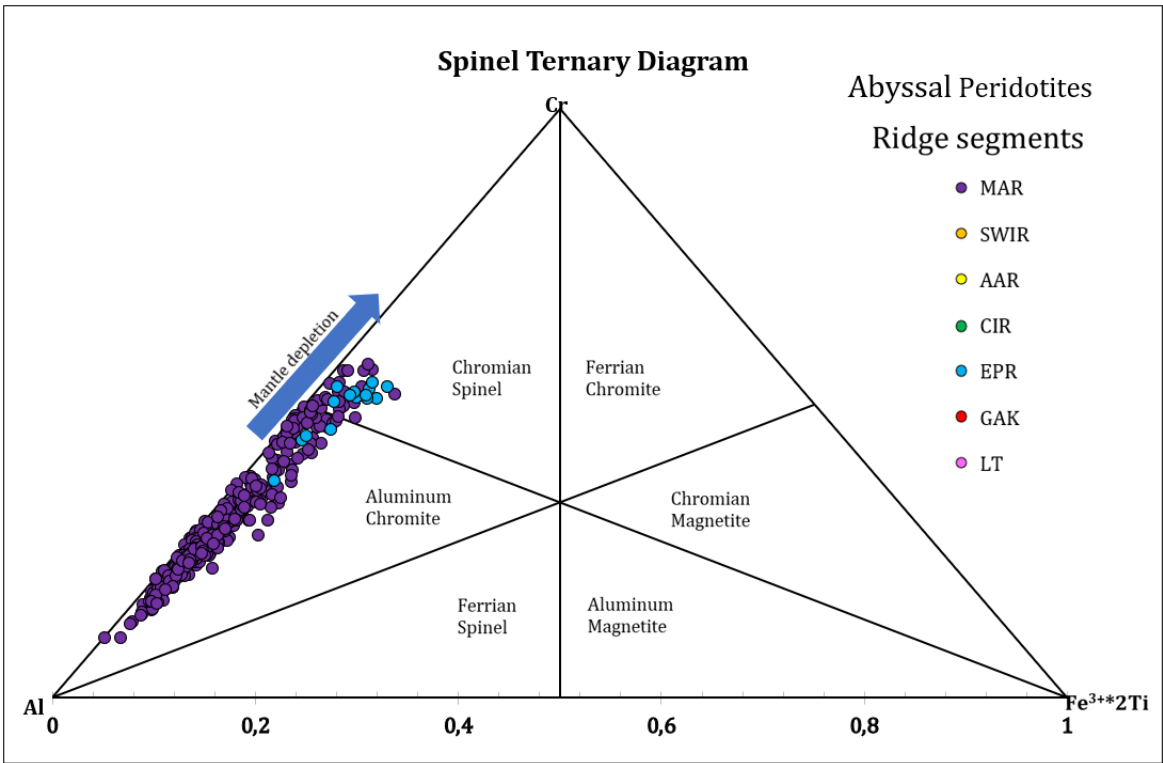


Figure 2: Spinel types in non-metasomatized EPR and MAR abyssal peridotites.

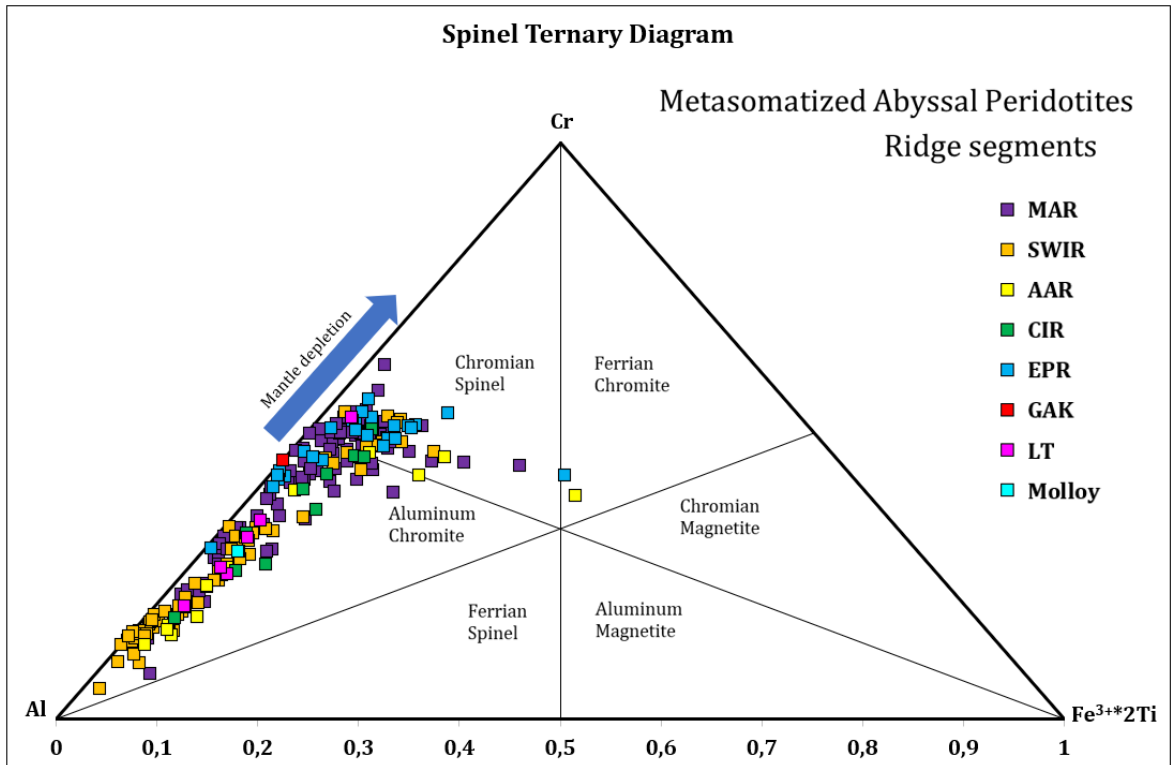


Figure 3: Spinel types in metasomatized abyssal peridotites.

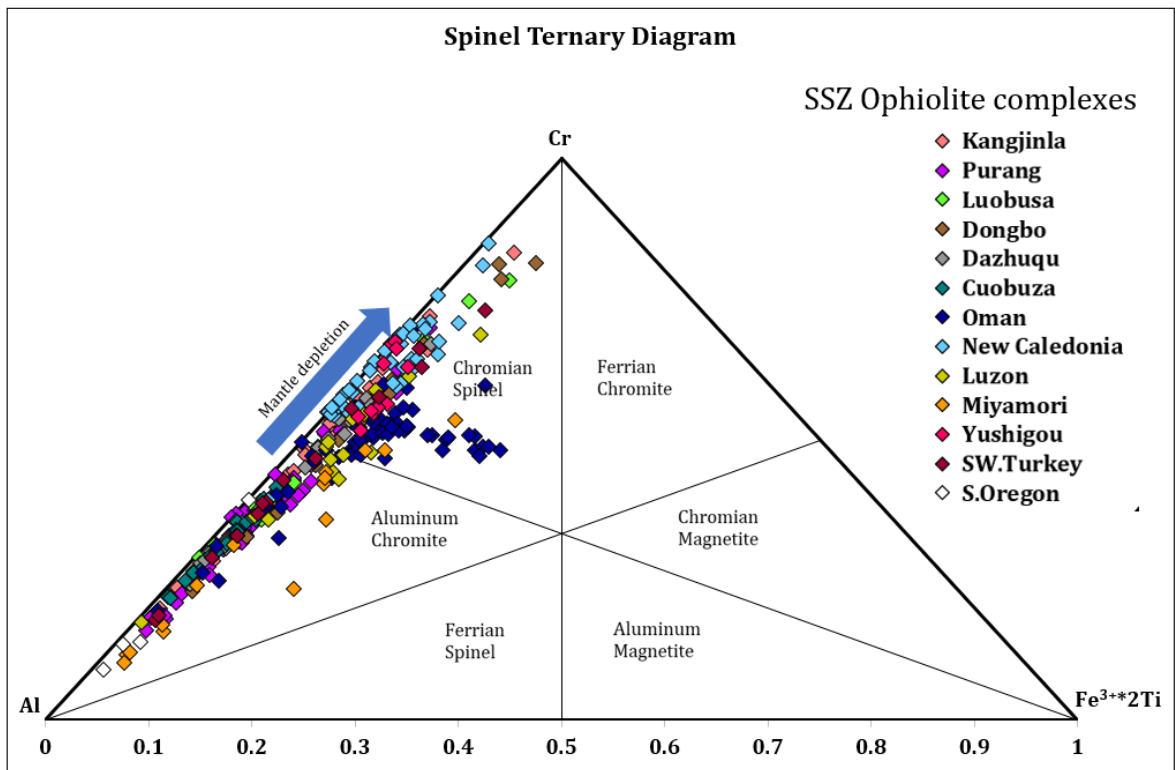


Figure 4: Spinel types in SSZ ophiolitic peridotites.

2.4 Peridotite characterization by olivine–spinel compositional relationship

To gain more insight, spinel Cr# and olivine Fo [(Mg/(Mg+Fe))] of peridotites were plotted onto an OSMA diagram (Figs. 5-7). The **Olivine–Spinel Mantle Array** was proposed by Arai (1984, 1990), to discriminate peridotites from various tectonic settings.

Figure 5 shows that for olivine Fo values ranging from 90-92, the spinel Cr# of non-metasomatized abyssal peridotites varies from 0.1-0.58. Values of Cr# <0.3 correspond to lherzolites indicating a more fertile mantle whereas the rest of the samples are mostly harzburgites. A couple of samples from MAR follow a trend of melt crystallization, which indicates melt infiltration. These specific samples were dredged from the Doldrums multi-fault transform system, and their Fo content, along that of all other samples with Fo<90, indicates non-mantle-derived olivine.

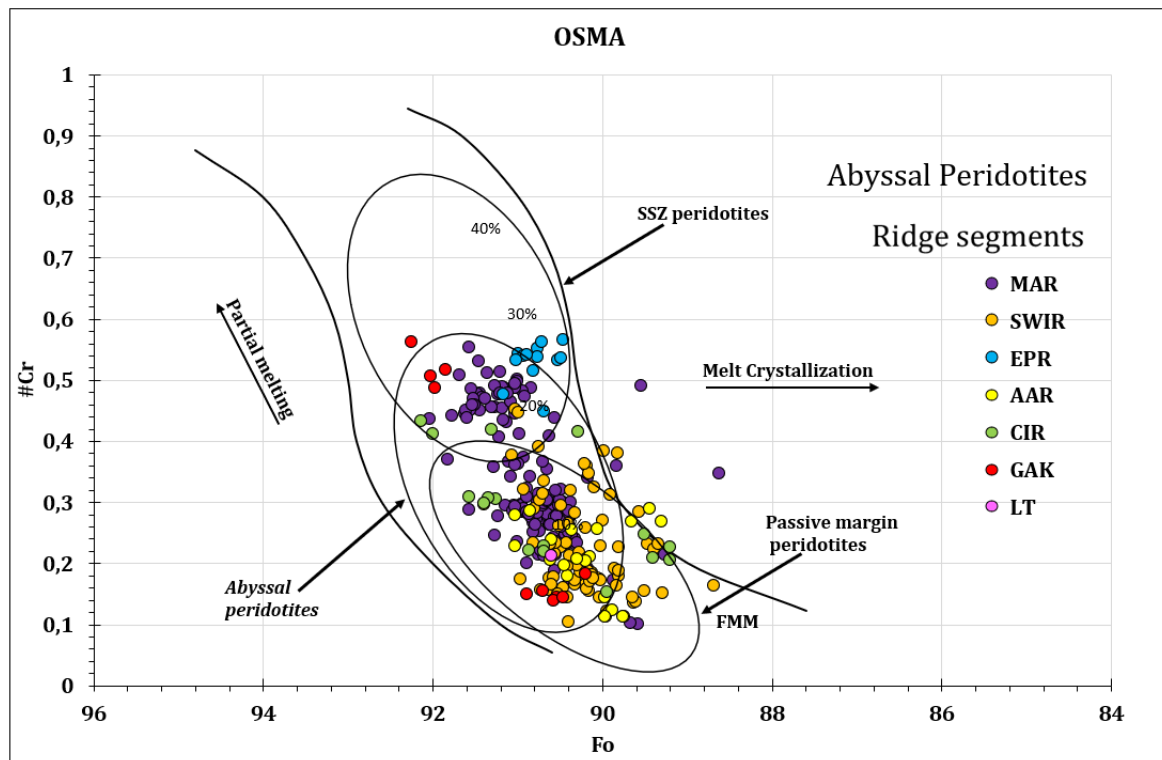


Figure 5: Olivine–Spinel Mantle Array, showing the correlation between spinel Cr# and olivine Fo in all non-metasomatized abyssal peridotite samples per ridge segment.

When considering metasomatized abyssal peridotites their olivine Fo content ranges from 92 to 90 and their spinel Cr# from 0.1- 0.6 (Fig. 6). There is a significant number of samples with Fo < 90 following the melt crystallization path. These samples indicate that their olivine is non-mantle derived. Low Fo also suggests that metasomatic melts/fluids depleted in Mg reacted with the rocks reducing their Fo content. The samples with spinel Cr# > 0.3 indicate a more depleted source. Samples with Fo content

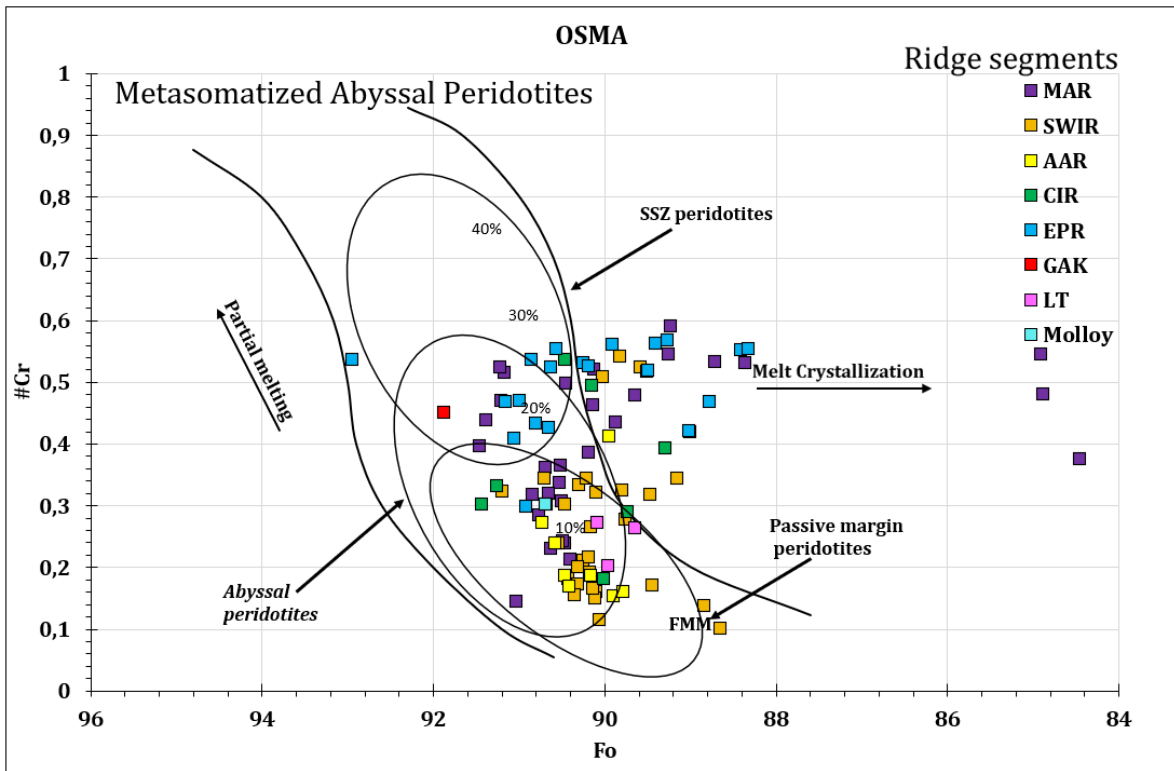


Figure 6: Olivine-Spinel Mantle Array, showing the correlation between spinel Cr# and olivine Fo in all metasomatized samples per ridge segment.

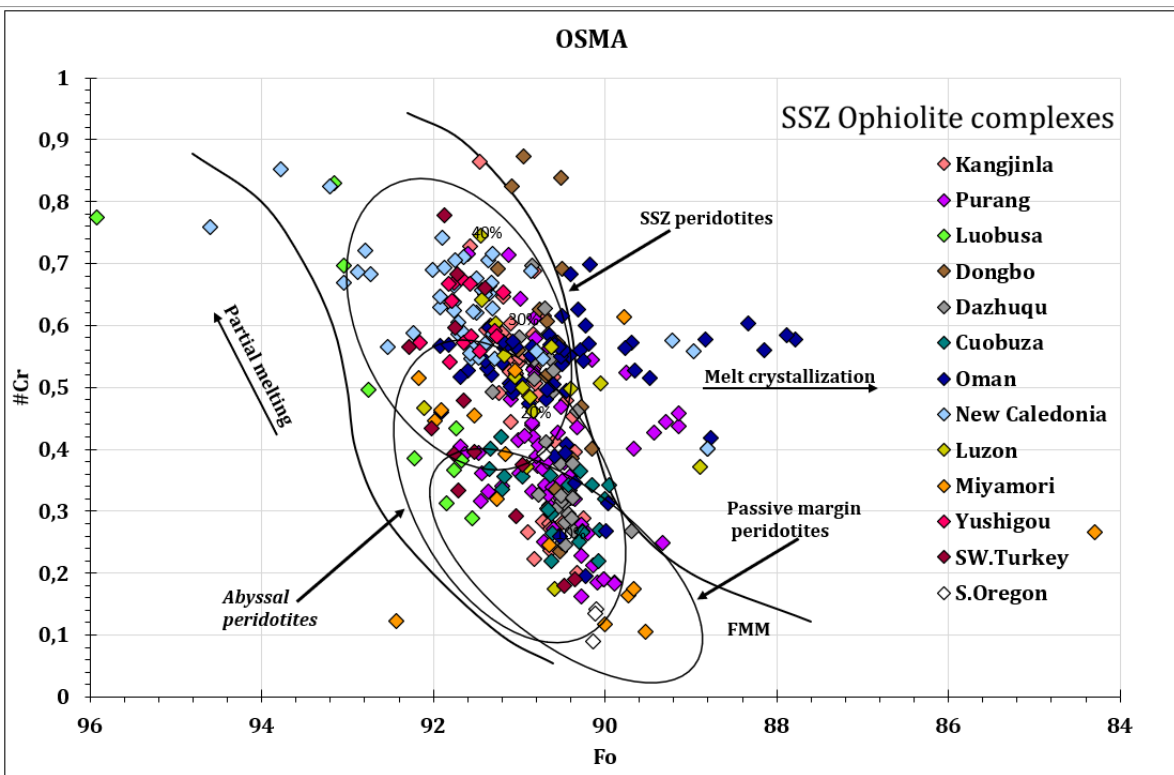


Figure 7: Olivine-Spinel Mantle Array, showing the correlation between spinel Cr# and olivine Fo in all SSZ peridotite samples per ophiolitic complex.

< 86, all come from the MAR and they are plagioclase harzburgites with gabbro veins. They have undergone melt infiltration from interacting with melts that crystallized plagioclase.

The ophiolitic SSZ peridotites, as shown on the Olivine-Spinel Mantle Array (Fig. 7), are the most depleted among all samples with spinel Cr# values up to 0.9, indicating that they have undergone extensive partial melting. A clear trend toward melt crystallization is also evident, particularly in the case of Oman, suggesting melt/fluid infiltration. Rare values of Fo>94 at comparable spinel Cr# indicate secondary (metamorphic) olivine from antigorite dehydration.

2.5. Spinel Al₂O₃ - TiO₂ systematics

Spinel Al₂O₃ and TiO₂ values are often used to constrain the nature of the mantle peridotite source (Bonatti & Michael, 1989), as they depend on mantle fertility but also on melt composition, which, in turn, is a function of pressure, temperature, and degree of partial melting. Therefore, the values of Al₂O₃ and TiO₂ in spinel for all peridotite samples were plotted on an Al₂O₃ vs TiO₂ diagram as a guide to tectonic provenance and magma chemistry (Figs. 8-10).

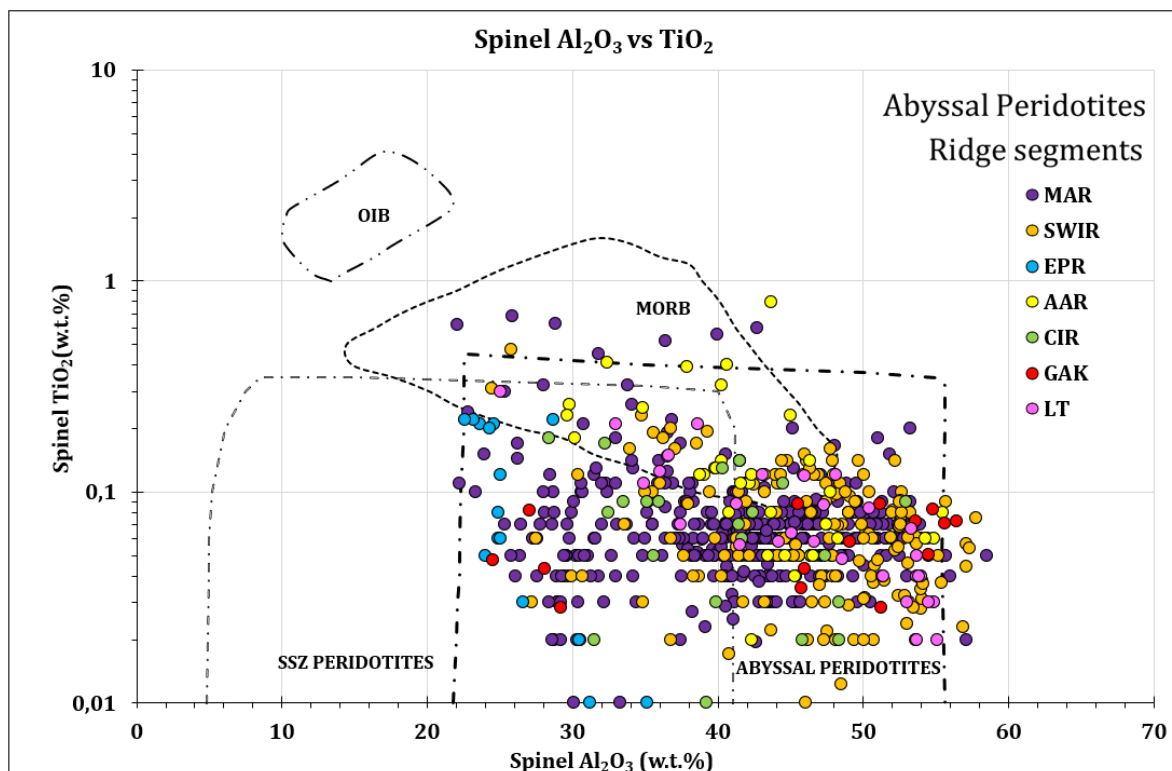


Figure 8: Spinel Al₂O₃ vs. TiO₂ for non-metasomatized abyssal peridotites.

In Fig. 8, the non-metasomatized abyssal peridotite spinels plot as expected in the abyssal peridotite field with some exceptions that plot in the MORB field. The samples with higher Ti content are from the MAR, specifically dredged from the Doldrums multi-fault transform system. These samples indicate MORB melt infiltration that changes their spinel chemistry and are considered a great indicator of metasomatic activity.

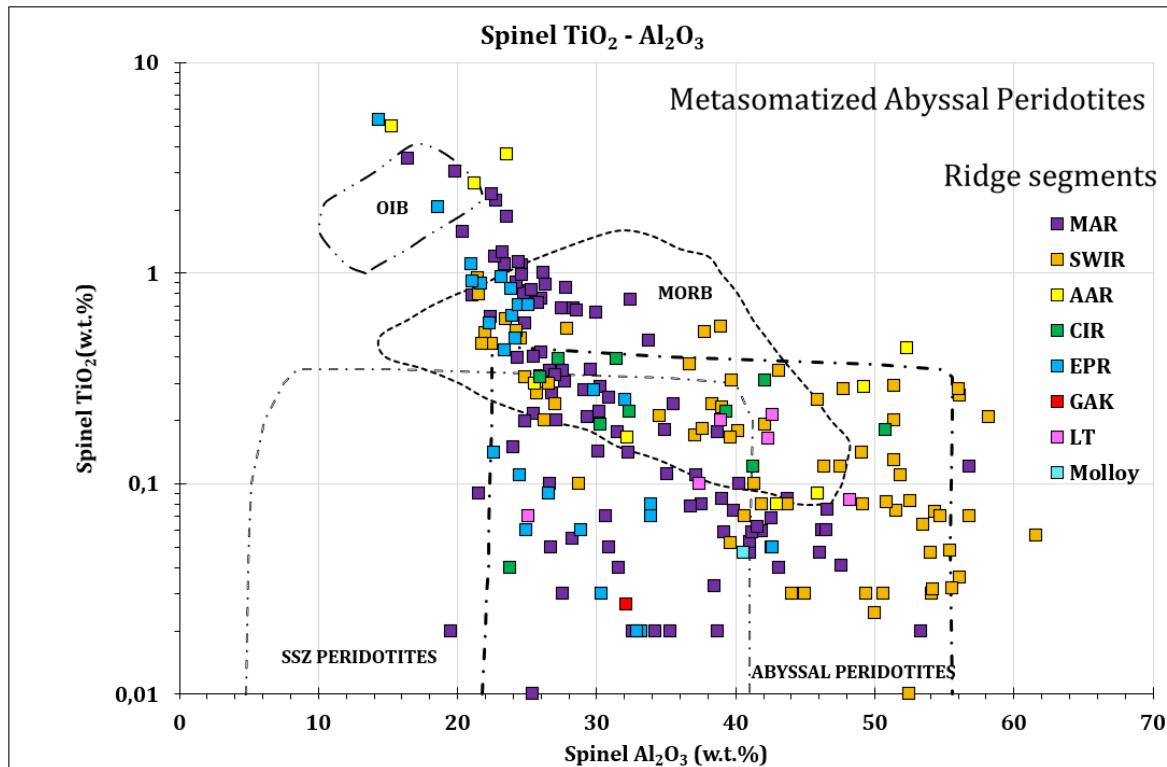


Figure 9: Spinel Al₂O₃ vs. TiO₂ for metasomatized abyssal peridotites.

As for the metasomatized abyssal peridotite spinels, they also plot in the field of abyssal peridotites, with many of them extending well into the MORB field (Fig. 9). The genesis of the samples (from MAR, SWIR, and EPR) that project into the MORB field could be ascribed to basaltic MORB-type melt percolation in the oceanic lithosphere and direct spinel crystallization from these melts. Few samples (from MAR, EPR, and AAR), display very high Ti contents and plot in the OIB field. They are Pl-harzburgites, Pl-dunites, Pl-wehrlites and gabbro-veined harzburgites and indicate infiltration of alkaline OIB melts causing metasomatism.

Spinel from ophiolitic SSZ peridotites plot across the entire SSZ and abyssal peridotite fields (Fig. 10). The samples that plot outside the SSZ peridotite and within the abyssal peridotite fields ($40 < \text{Al}_2\text{O}_3 < 60$ wt.%) most likely represent trapped, relatively primitive oceanic mantle onto which the SSZ sequence was built. The samples from New Caledonia are the most depleted among all SSZ ophiolites, having very low alumina and titania

contents. Certain samples from Oman, project near the OIB field suggesting infiltration metasomatism by OIB-like melts. These specific samples are all wehrlites with very high Ti contents due to melt metasomatism.

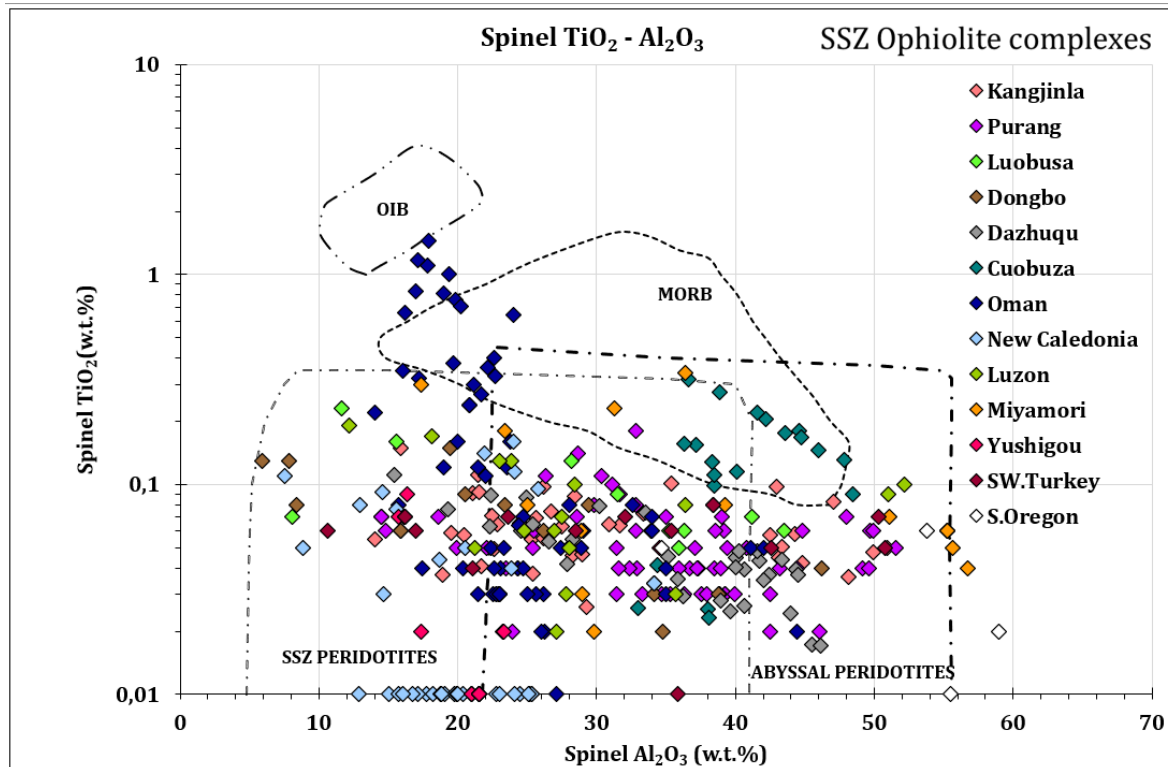


Figure 10: Spinel Al₂O₃ vs. TiO₂ for ophiolitic SSZ peridotites.

2.6 Spinel Ti - Cr# systematics

Spinel Ti and Cr# systematics was explored to determine the degree of melting and the provenance of spinel (Figs. 11-13). The degree of melting (F) was calculated using the equation: $F = 10 \ln(Cr\#) + 24$ (Hellebrand et al., 2001). Most non-metasomatized abyssal peridotite spinels suggest melting up to 15%, whereas there are certain samples that have experienced melting larger than 15% (mainly from MAR and EPR) suggesting that they are the most depleted (Fig. 11). These are the same samples that were identified in other diagrams as well (e.g. Figs. 2 & 5) as having derived of a more depleted mantle. High Ti contents in a few samples (from MAR and AAR) imply that the spinels are products of metasomatism, which was also seen in Fig.8.

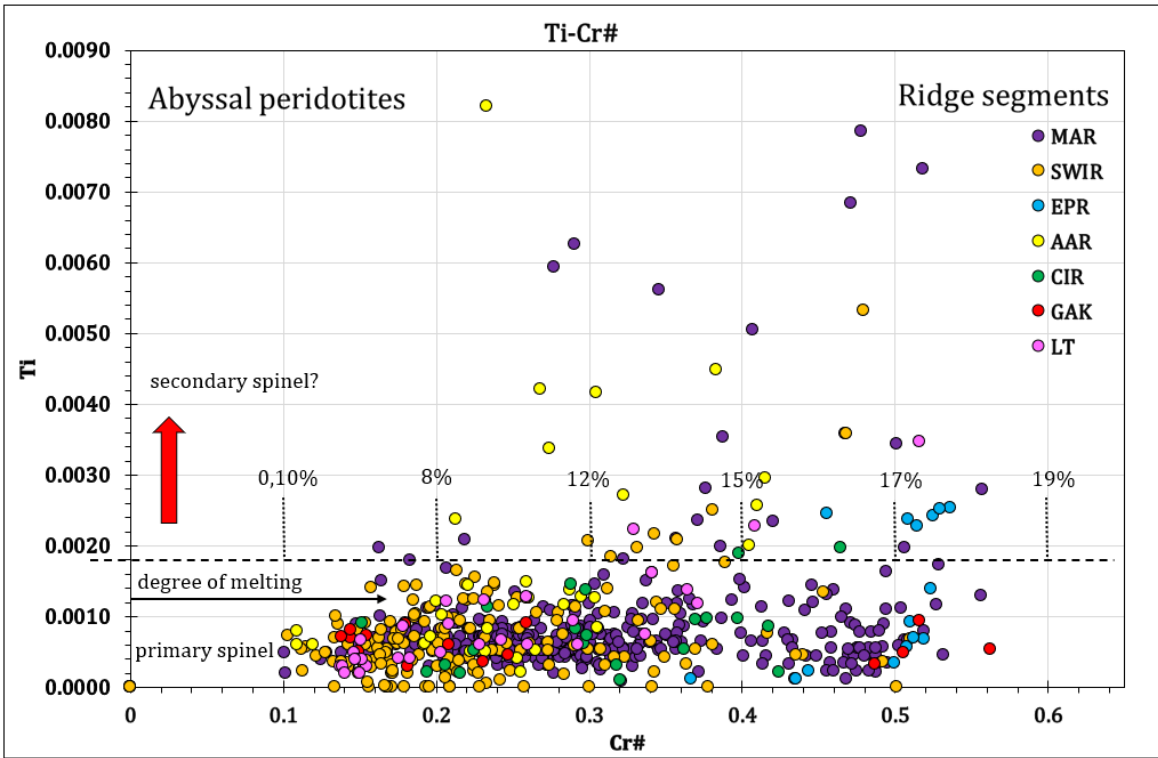


Figure 11: Spinel Ti vs. Cr# of non-metasomatized abyssal peridotites.

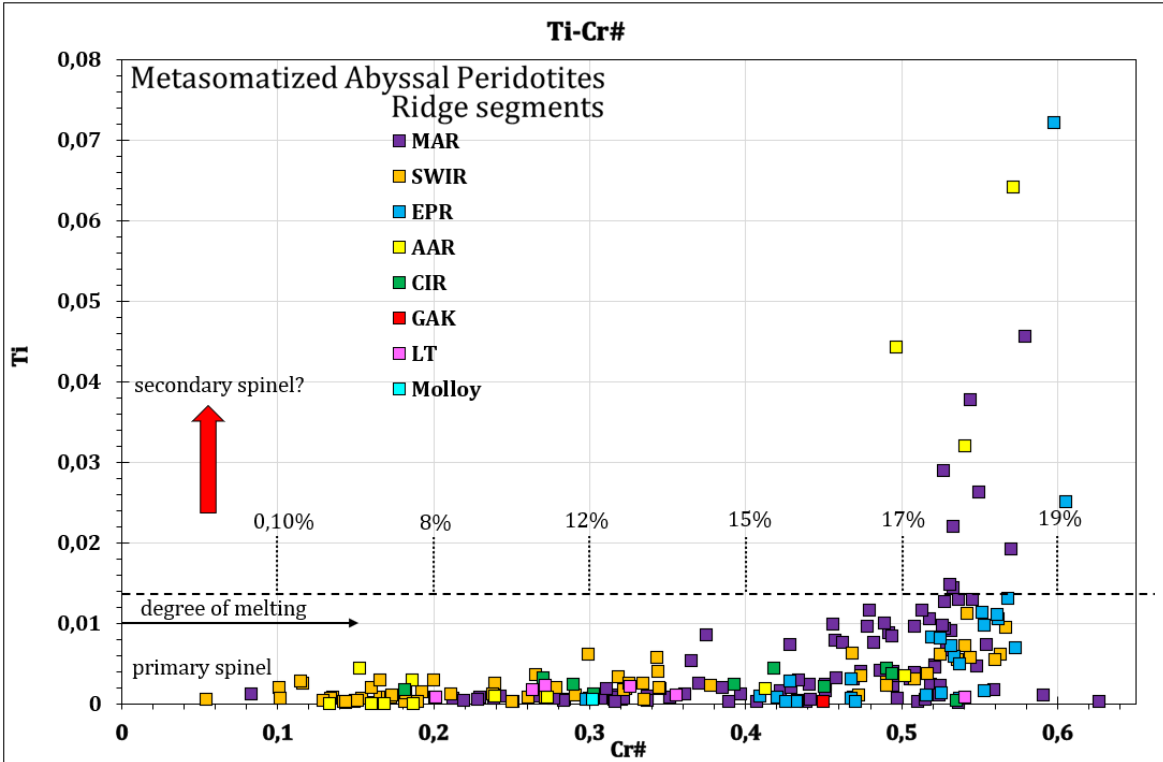


Figure 12: Spinel Ti vs. Cr# of metasomatized abyssal peridotites.

Spinel from metasomatized abyssal peridotites are more depleted than those from non-metasomatized ones (Cr# values up to 0.6; Fig. 12). Significantly, the samples with the highest Cr# also display the highest Ti values suggesting either infiltration-induced melting or percolation of enriched melts in and chemical interaction with a depleted source. The samples (from MAR, EPR, and AAR) with high Ti contents, were identified in Fig.14 as projecting onto the OIB field, suggesting OIB melt infiltration and metasomatism.

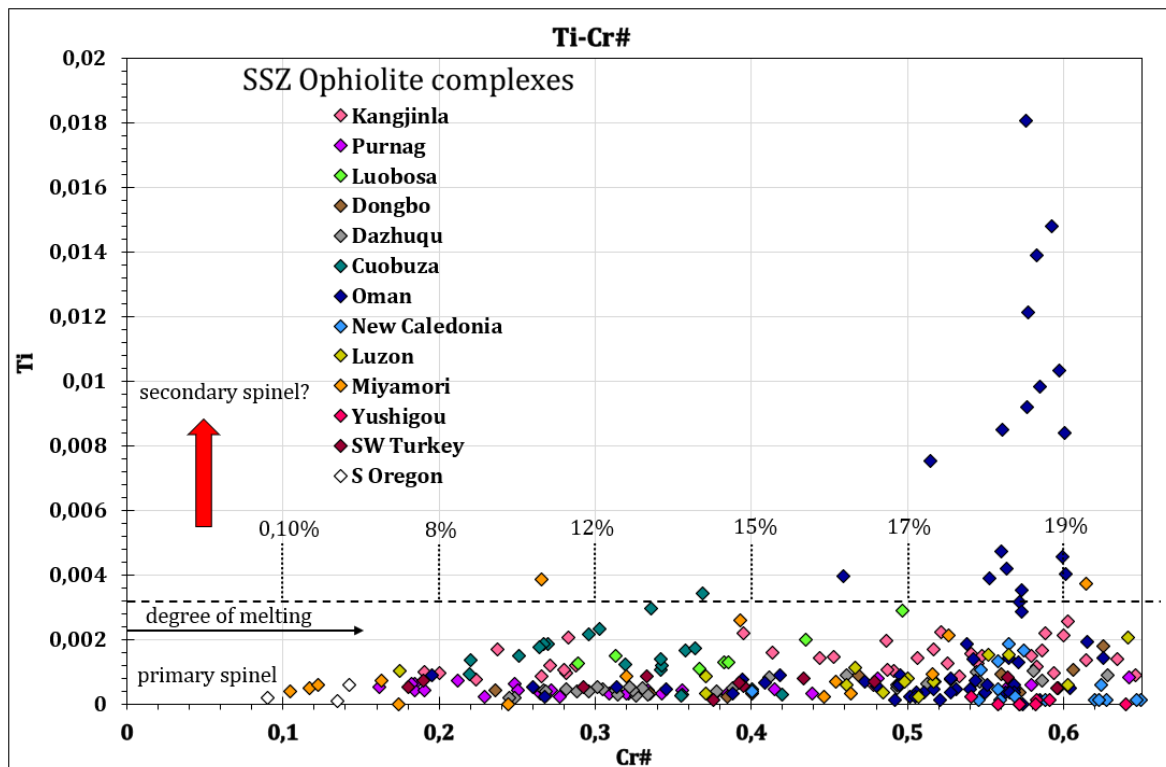


Figure 13: Spinel Ti vs. #Cr of ophiolitic SZZ peridotites.

Spinel from SZZ ophiolitic peridotites are the most depleted among all samples with a degree of melting reaching up to 19%. The samples with the higher Ti contents are all from Oman. These specific samples indicate secondary spinel and melt infiltration. These samples as shown in Fig.10, plot near the OIB field pointing to OIB alkaline melt infiltration.

3. Thermometry and Oxybarometry

3.1. Introduction to geothermometry

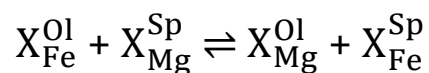
Geothermometry in petrology is the use of chemical information (compositions of minerals and rocks in equilibrium) and its transformation via thermodynamics to physical information (temperature of equilibration), provided that pressure is known or can be estimated. Mineral geothermometry is governed by cation exchange between minerals in equilibrium. The obtained temperature reflects, in effect, the closure temperature of the cations in the minerals considered to diffusion, and is a function of cooling rate and time.

Geothermometry is a powerful tool to determine the thermal history of a rock. It can also be applied to geothermal exploration to estimate subsurface temperatures, which is crucial for assessing the feasibility of geothermal energy production. Geothermometry is extremely important in mineral exploration, as knowing the timing and temperature of ore deposition is crucial in successful drilling.

3.2 Olivine-Spinel thermometry – Thermodynamic background

One important geothermometer for shallow upper mantle peridotites like those studied in the present thesis is the olivine-spinel geothermometer. It is based on the Fe^{2+} - Mg^{2+} cation exchange between olivine $(Mg, Fe^{2+})_2 SiO_4$ and spinel $(Mg, Fe^{2+}) (Al, Cr, Fe^{3+})_2 O_4$.

This exchange can be simply written as:



The equilibrium constant is:

$$K_D = \frac{X_{Fe}^{Sp} X_{Mg}^{Ol}}{X_{Mg}^{Sp} X_{Fe}^{Ol}}$$

where X_i^a is the mole fraction of component i in phase a.

At equilibrium, the difference in Gibbs free energy between the products and the reactants is zero:

$$\Delta G = \Delta H + P\Delta V - T\Delta S \Rightarrow 0 = \Delta H + P\Delta V - T\Delta S + RT\ln K_D \Rightarrow T = \frac{\Delta H + P\Delta V}{RT\ln K_D - \Delta S}$$

G	Gibbs free energy (J)
H	Enthalpy (J/mol)
V	Volume (J/mol/bar)
S	Entropy (J/mol/K)
P	Pressure (bar)
K _D	Equilibrium constant
R	Gas constant (J/mol/K)
T	Temperature (K)

Literature estimates of equilibration temperatures for olivine-spinel pairs in ultramafic complexes fluctuate between 700°C and 900°C. Temperatures calculated using Mg-Fe exchange between coexisting orthopyroxene and clinopyroxene, where applicable, in these rocks are considerably higher because of higher closure temperatures of these cations in pyroxenes.

The equilibrium exchange of Fe and Mg between olivine and spinel is the fastest among other mineral pairs in peridotites and continues efficiently during the cooling down to relatively low temperatures, while the pyroxene thermometers are blocked at higher temperatures.

3.3 Olivine-Spinel thermometry - Applications

3.3.1 The BBG91 geothermometer

The BBG91 olivine-spinel geothermometer was constructed by Ballhaus et al. (1991) and is an improved version of an older calibration of the thermometer first presented by O'Neill and Wall (1987). Ballhaus et al. (1991) showed that the O'Neill and Wall (1987) geothermometer tends to underestimate run temperatures progressively with decreasing spinel Cr#. They further identified the same systematic relationship when the O'Neill and Wall (1987) thermometer was applied to Cr - Al spinels from mantle xenoliths (Fig. 14). The BBG91 thermometer is given by the equation:

$$T = \left(6530 + 280P + (7000 + 108P) * (1 - 2X_{Fe}^{Ol}) - 1960 * (X_{Mg}^{Sp} - X_{Fe^{2+}}^{Sp}) + 16150 * X_{Cr}^{Sp} + 25150 * (X_{Fe^{3+}}^{Sp} + X_{Ti}^{Sp}) \right) / \left(R \ln K_{Mg-Fe}^{Ol-Sp} + 4.705 \right)$$

where T is in K, P is in GPa, $X_{Fe^{3+}}^{Sp} = Fe^{3+}/\Sigma R^{3+}$ in spinel, X_{Fe}^{Ol} and $X_{Fe^{2+}}^{Sp}$ the $Fe^{2+}/(Fe^{2+} + Mg)$ ratios in olivine and spinel, $X_{Cr}^{Sp} = Cr/\Sigma R^{3+}$ in spinel, X_{Ti}^{Sp} is the number of Ti cations in spinel to 4 oxygens.

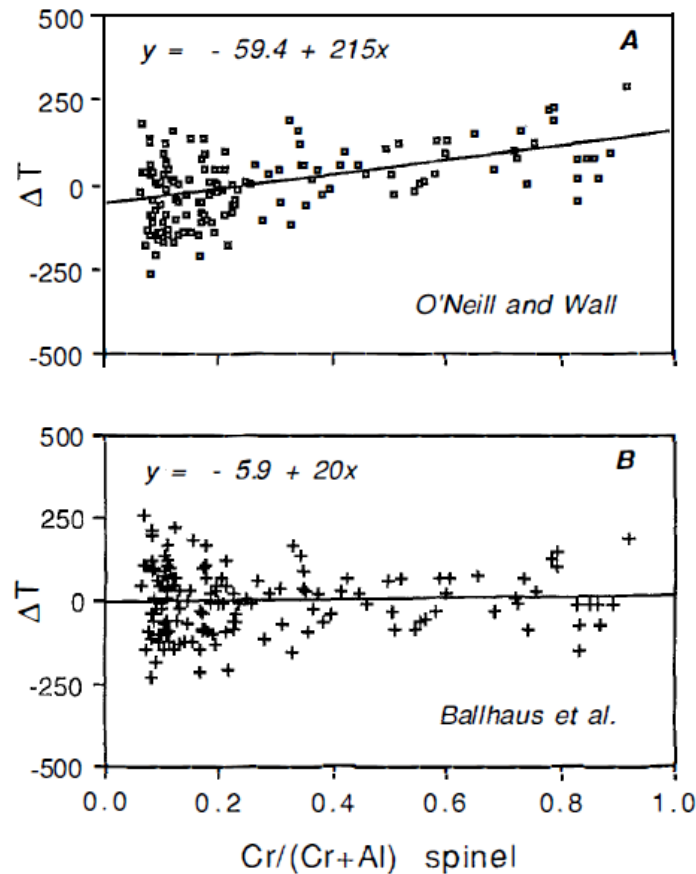


Figure 14: Comparison between the O'Neill and Wall's (1987) thermometer (A) and the BBG91 thermometer (B). ΔT is the deviation of calculated temperatures from the mean Ol-Sp temperature of 154 Ol-Sp pairs from spinel lherzolite xenoliths worldwide, plotted against $Cr/Cr+Al$ in spinel.

3.3.2 The LKVF95 geothermometer

The LKVF95 olivine-spinel geothermometer is a newer calibration of the Ol-Sp formulation of Fabriés (1979). The latter was based upon several sets of data which were reexamined by Li et al., 1995 who concluded that the data were unworthy giving lower temperatures than expected.

Fabriés (1979) calibrated his 700°C isotherm using natural peridotite ol-sp pairs taken from Medaris (1975). assuming they had equilibrated at the prescribed temperature. His 1225°C isotherm was inferred from the Fe/Mg ratio of glass in equilibrium with olivine

from the eruption of the Kilauea Iki volcano in 1959. Evans et al. (1972) considered this temperature as the equilibration temperature between olivine and spinel phenocrysts. However, since spinel and olivine are the subliquidus phases, these minerals had obviously crystallized at a temperature higher than the eruption temperature. The experimental data of Mori (1977) was used by Fabriés (1979) to establish the 1200°C isotherm. The spinel analysis used was nevertheless contaminated by clinopyroxene which was much poorer in FeO (2.56 w.t.%) compared to the coexisting spinel (10.49 w.t.%), leading to an erroneous K_D value. Lastly, Fabriés (1979) used the experimental work of Mysen et al. (1975) that was criticized for severe iron loss from the charge to the capsule and disequilibrium Ol and Sp compositions. Therefore, the reference temperatures and/or the Fe-Mg Ol-Sp K_D values used by Fabriés (1979) needed to be reevaluated due to their uncertainty.

The improved calibration of the Fabriés (1979) thermometer proposed by Li et al. (1995) is depicted graphically in Fig. 15 and described by the following equation:

$$T (^{\circ}\text{K}) = \frac{4299 Y_{\text{Cr}}^{\text{Sp}} + 1283}{\ln K_d^0 + 1.469 Y_{\text{Cr}}^{\text{Sp}} + 0.363}$$

where $\ln K_d^0 = \ln \frac{X_{\text{Mg}}^{\text{Ol}} X_{\text{Fe}}^{\text{Sp}}}{X_{\text{Fe}}^{\text{Ol}} X_{\text{Mg}}^{\text{Sp}}} - 2.0 Y_{\text{Fe}^{3+}}^{\text{Sp}}$.

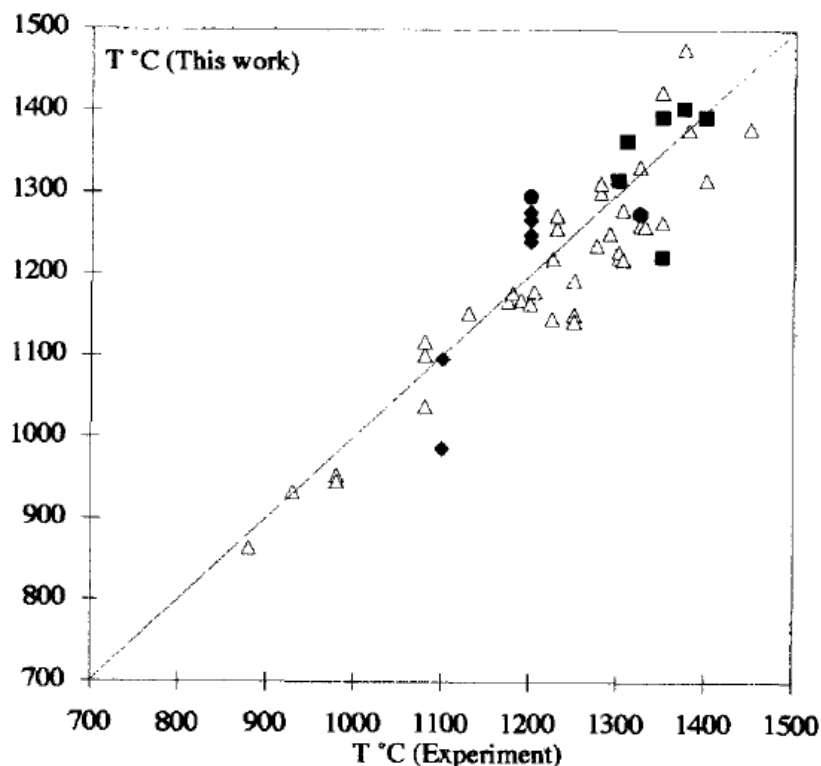


Figure 15: Comparison between temperatures calculated by LKVF95 geothermometer compared with experimental temperatures (Li et al., 1995).

The correlation between temperatures calculated with the LKVF95 geothermometer and experimental temperatures is rather linear indicating that LKVF95 is reliable based on the good fit between the two parameters.

3.3.3 Comparison between the BBG91 and LKVF95 geothermometers

To compare the two most cited Fe-Mg Ol-Spl thermometers in the geological literature, the experimental data of Ballhaus et al. (1991) were used to calculate temperatures using the formula of Li et al. (1995) and vice versa . The results are plotted as Figure 16. The BBG91 thermometer underestimates the experimental temperatures of Li et al. (1995) by approximately 250°C on average, whereas the LKVF95 thermometer overestimates the experimental temperatures of Ballhaus et al. (1991) by approximately 100°C on average. The reason for such a huge discrepancy between the two calibrations is not clear at all, however the LKVF95 equation appears to predict temperatures more accurately as a number of experiments plot along the 1:1 line.

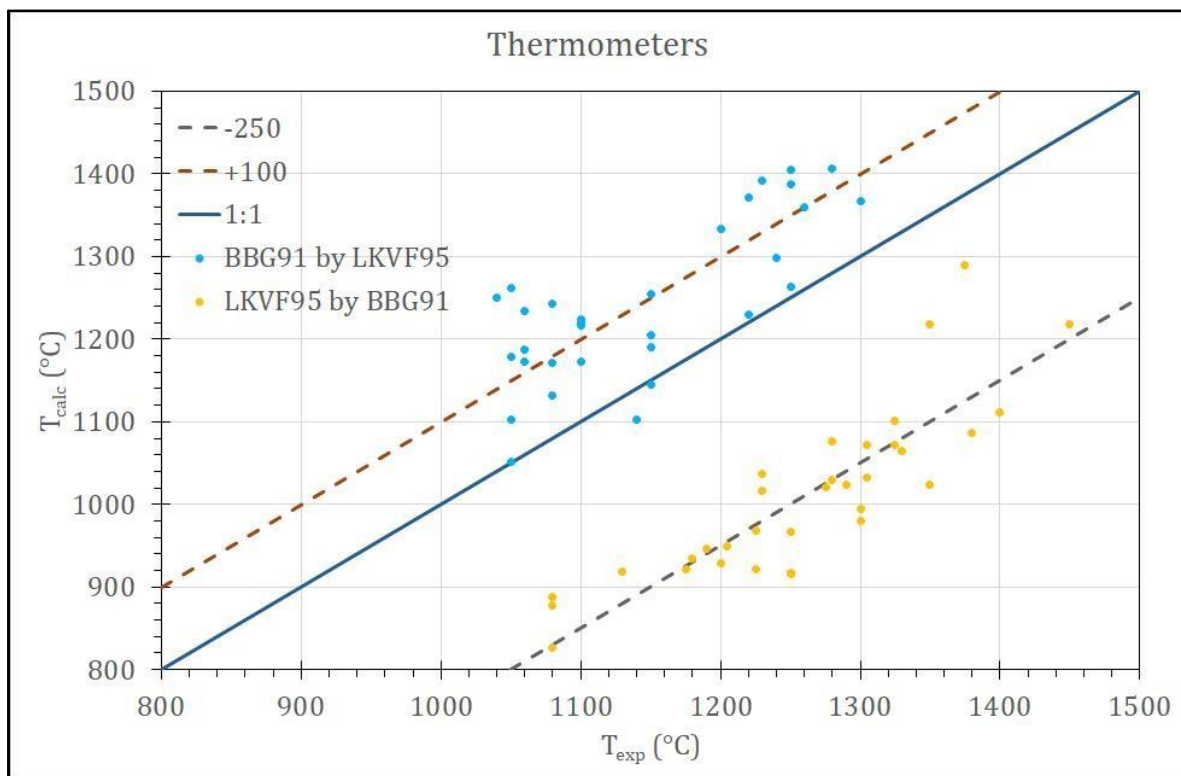


Figure 16: Temperatures calculated with the BBG91 thermometer using the experimental data of LKVF95 and vice versa plotted against their respective experimental temperatures.

To further evaluate the temperatures obtained from the two geothermometers, a comparison of temperature calculated using the two calibrations was conducted across all three data sets used in this thesis (Figs. 17-19).

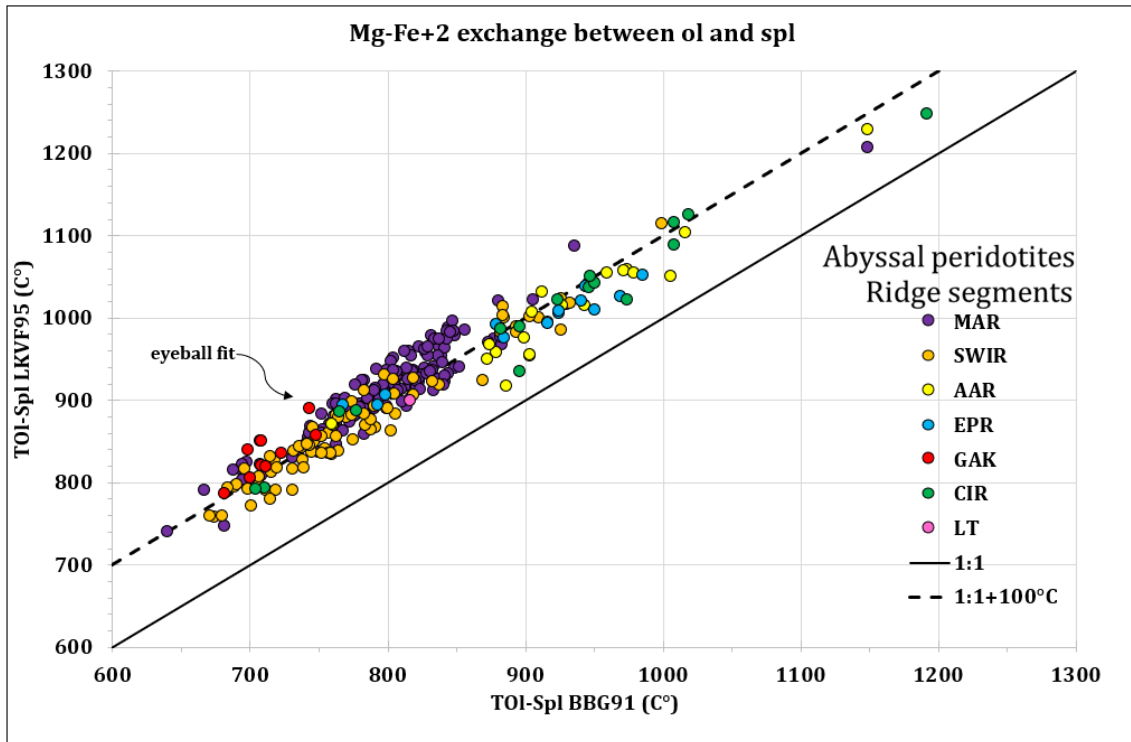


Figure 17: Temperatures calculated with the LKVF95 geothermometer plotted against temperatures calculated with the BBG91 geothermometer for non-metasomatized abyssal peridotites.

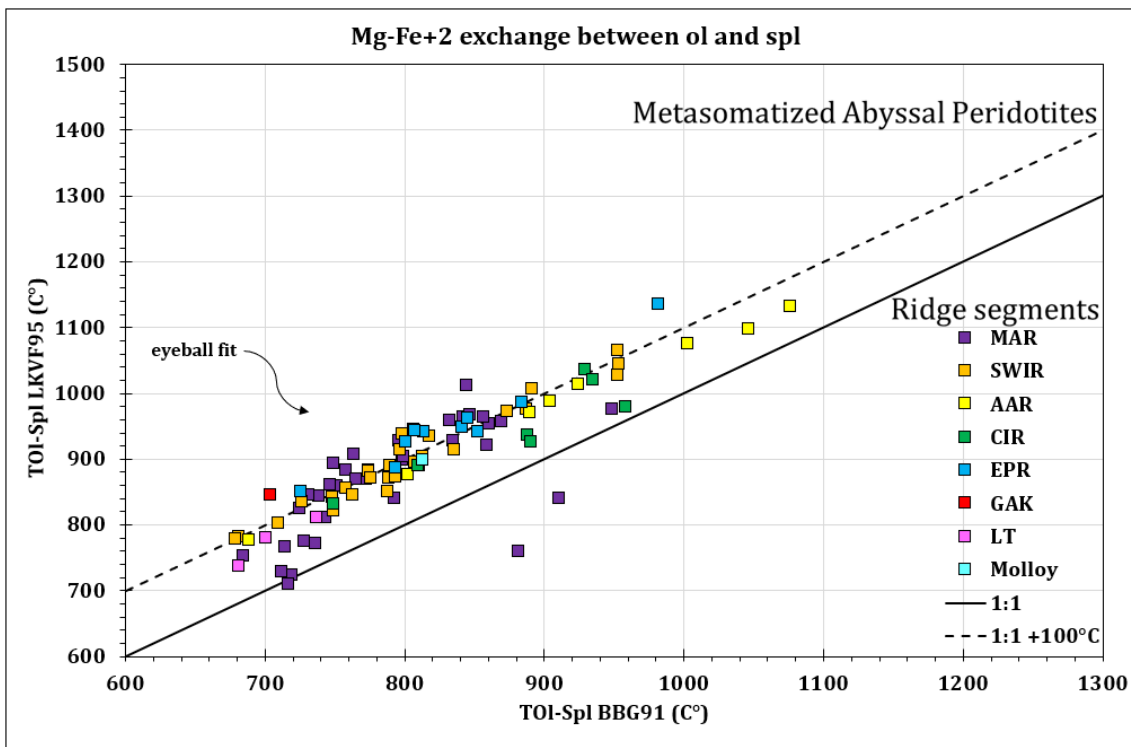


Figure 18: Temperatures calculated with the LKVF95 geothermometer plotted against temperatures calculated with the BBG91 geothermometer for metasomatized abyssal peridotites.

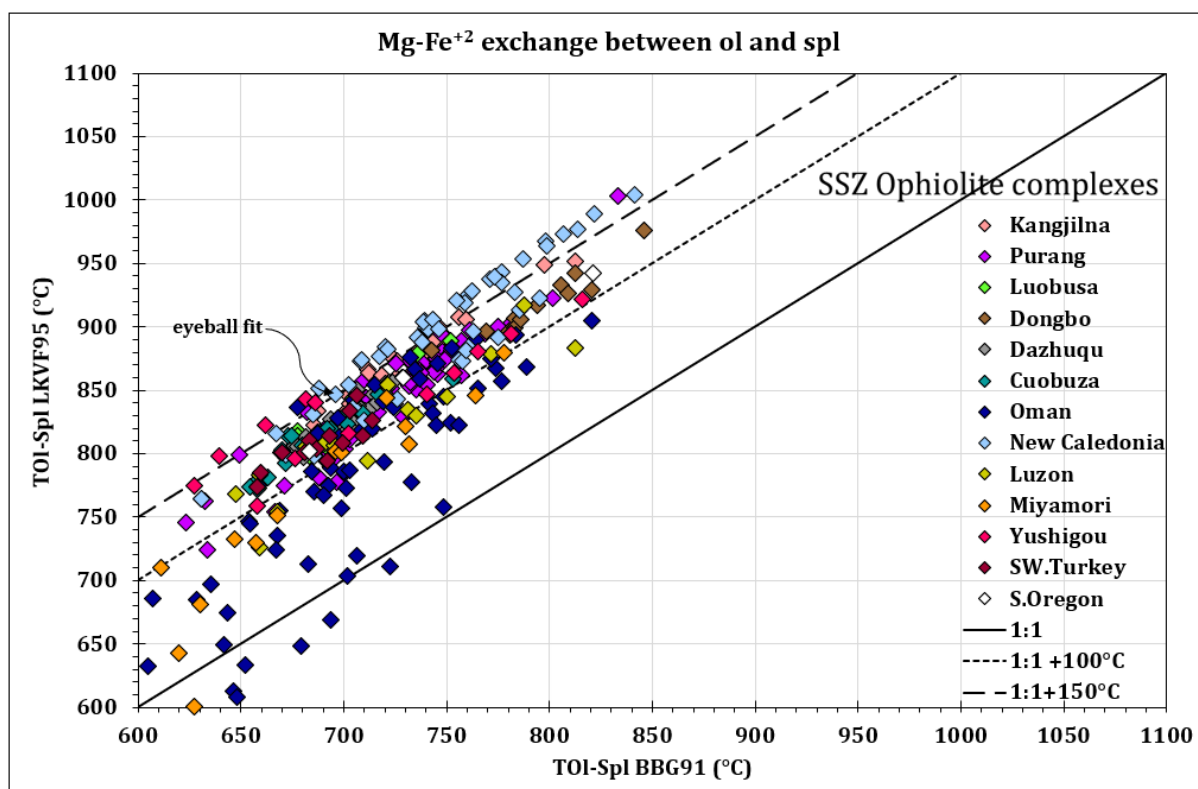


Figure 19: Temperatures calculated with the LKVF95 geothermometer plotted against temperatures calculated with the BBG91 geothermometer for SSZ ophiolitic peridotites.

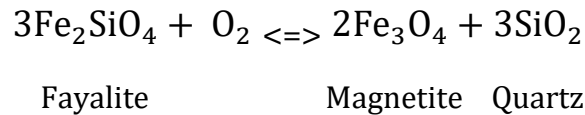
Inspection of Figs. 17-19 reveals that LKVF95 temperatures are higher than BBG91 temperatures by 100°C for abyssal peridotites and by 100-150°C for ophiolitic SSZ peridotites. Only some highly metasomatized Oman peridotites display a 1:1 correlation. In the remainder of this thesis, all ol-spl temperature calculations will be performed using the LKVF95 calibration.

3.4 Oxybarometry and the redox state of the upper mantle

Oxygen fugacity (fO_2) is a fundamental but little-known intensive variable in mantle processes (Ballhaus et al., 1991). Mantle fO_2 has wide-ranging implications for many Earth-system processes (Sorbadère et al., 2018), and has been estimated based on mineral oxybarometers (O’Neil and Wall, 1987, Ballhaus et al., 1991, Davis et al., 2017). To begin with, fO_2 can influence the stability of minerals, for instance, fO_2 changes can shift the stability boundaries between minerals, leading to the formation or breakdown of specific minerals. Another process where oxygen fugacity takes a significant place is during magma generation and differentiation as magma’s viscosity and the behavior of volatile elements are highly influenced by fO_2 . Oxygen fugacity is also fundamental for redox reactions and element partitioning of fluids degassed from mantle-derived melts. High values of fO_2 are more likely to produce CO_2 and H_2O , whereas lower fO_2 values

produce CO, CH₄, and H₂. Redox reactions are the ones where elements change their oxidation state affecting their partitioning between minerals; the redox state refers to the balance between oxidized and reduced species in a system.

Minerals coexist because of a redox exchange as mentioned above. The presence of certain minerals together constitutes an oxygen buffer, where a fugacity of O₂ dependent on T and P must be present. The Fayalite-Magnetite-Quartz (FMQ) buffer is used as a reference state.



Regarding the redox state of the suboceanic mantle, the $f\text{O}_2$ is on average 0.9 ± 0.7 log units below the FMQ buffer, whereas the subcontinental mantle is by far more oxidized, for which the average value of $f\text{O}_2$ is approximately 0.24 ± 0.5 log units above the FMQ buffer (Bryndzia, Wood, 1990).

The $f\text{O}_2$ of all samples mentioned in this thesis was calculated with the olivine-orthopyroxene-spinel oxygen geobarometer calibrated by Ballhaus et al., 1991.

The calibration of the oxygen geobarometer is given by the following equation:

$$\Delta \log(f\text{O}_2)^{FMQ} = 0.27 + 2505/T - 400P/T - 6 \log(X_{Fe}^{Ol}) - 3200(1 - X_{Fe}^{Ol})^2/T + 2 \log(X_{Fe^{2+}}^{Sp}) + 4 \log(X_{Fe^{3+}}^{Sp}) + 2630(X_{Al}^{Sp})^2/T$$

where T is in K, P is in GPa, $X_{Fe^{3+}}^{Sp} = Fe^{3+}/\Sigma R^{3+}$ in spinel, $X_{Al}^{Sp} = Al/\Sigma R^{3+}$ in spinel, X_{Fe}^{Ol} and $X_{Fe^{2+}}^{Sp}$ the $Fe^{2+}/(Fe^{2+} + Mg)$ ratios in olivine and spinel.

3.5 Redox state of spinel peridotites according to their Cr# in correlation with temperature

Oxygen fugacity, a measure of the partial pressure of oxygen in a given environment, plays a pivotal role in controlling the oxidation-reduction reactions within the mantle. As mantle rocks undergo various tectonic and magmatic processes, temperature changes can significantly impact their redox state. Chromium (Cr), a trace element in mantle minerals, has been identified as a useful factor for monitoring redox conditions.

Understanding the Cr# $\left(\frac{Cr^{3+}}{Cr^{3+} + Al^{3+} + Fe^{3+}}\right)$ value in spinels can be helpful in the interpretation of the geological history of the rocks, regarding their redox conditions, as the Cr ratio reflects whether the environment was more reducing or oxidizing during mineral formation. Higher Cr# values (more Cr³⁺) are associated with reducing conditions, where there is a lack of oxygen. On the other hand, lower Cr# values (more

Cr⁺²) indicate a more oxidized environment, where oxygen is more prevalent (Ballhaus, 1993).

In this chapter, the redox state of the upper mantle is examined as indicated by variations in fO_2 , Cr#, and T_{ol-spl} calculated by the LKVF95 geothermometer. The fO_2 of each data set is plotted against Cr# and T_{ol-spl} to correlate how oxygen fugacity changes based upon closure temperatures of Fe-Mg exchange between olivine and spinel and Cr# (Figs. 20-23).

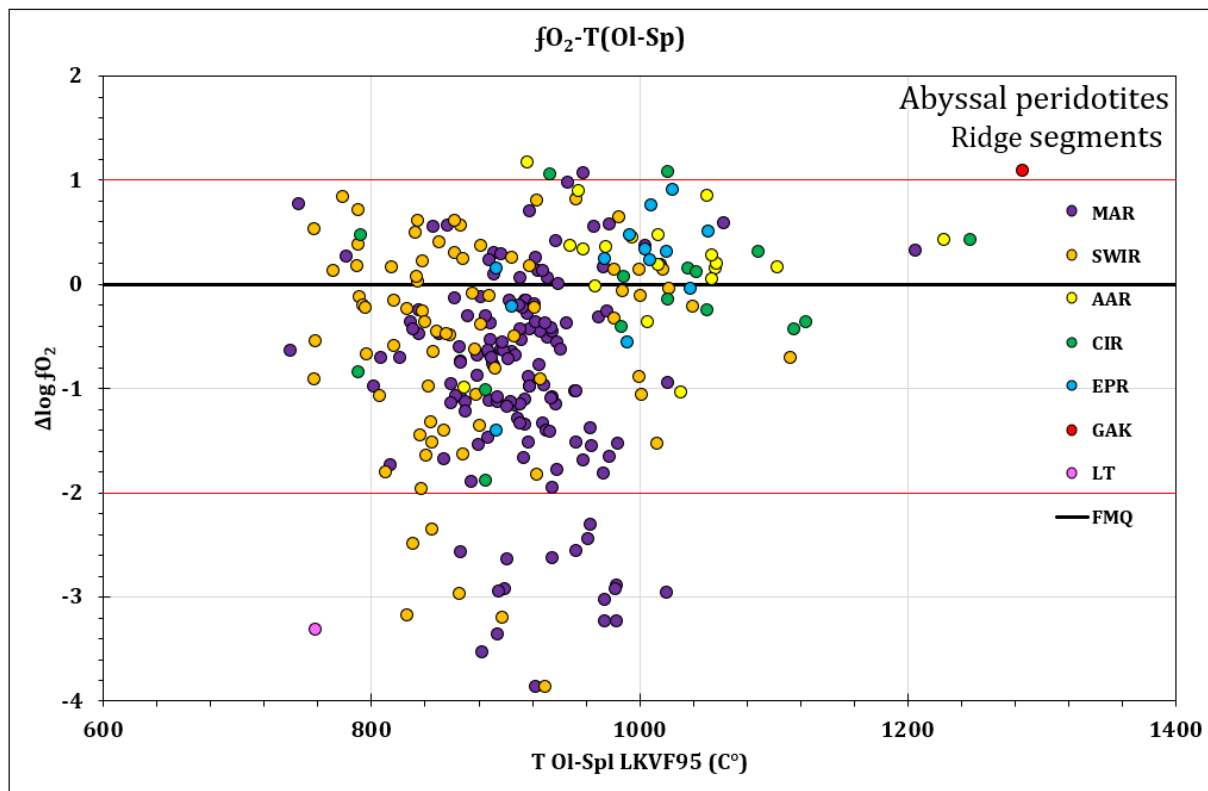


Figure 20: fO_2 given in log units relative to the FMQ equilibrium, plotted against T_{ol-spl} calculated with the LKVF95 geothermometer. The red lines indicate the range of fO_2 values that are representative of the upper mantle.

According to Figures. 20 & 21, the abyssal peridotites indicate a more reduced environment with a relative fO_2 range from FMQ-2 to FMQ. Their Cr# varies from 0.1 to 0.4 for most of the samples, representative of a more fertile mantle. The average temperatures of equilibration among these samples range between 800°C and 1000°C. Among the samples there is also a minority that plots at temperatures above 1000°C. The higher temperatures of the Ol-Spl geothermometer indicate that diffusion was blocked early during cooling due to fast emplacement.

Regarding metasomatized abyssal peridotites, their majority indicate a reduced environment overall, with an fO_2 range from FMQ-2 to FMQ+1 (Figs. 22 & 23). Their Cr#, varies from 0.1 to 0.6, with the higher Cr# values indicating a more reduced environment. A small group of samples display fO_2 values between FMQ+1 and FMQ+2.

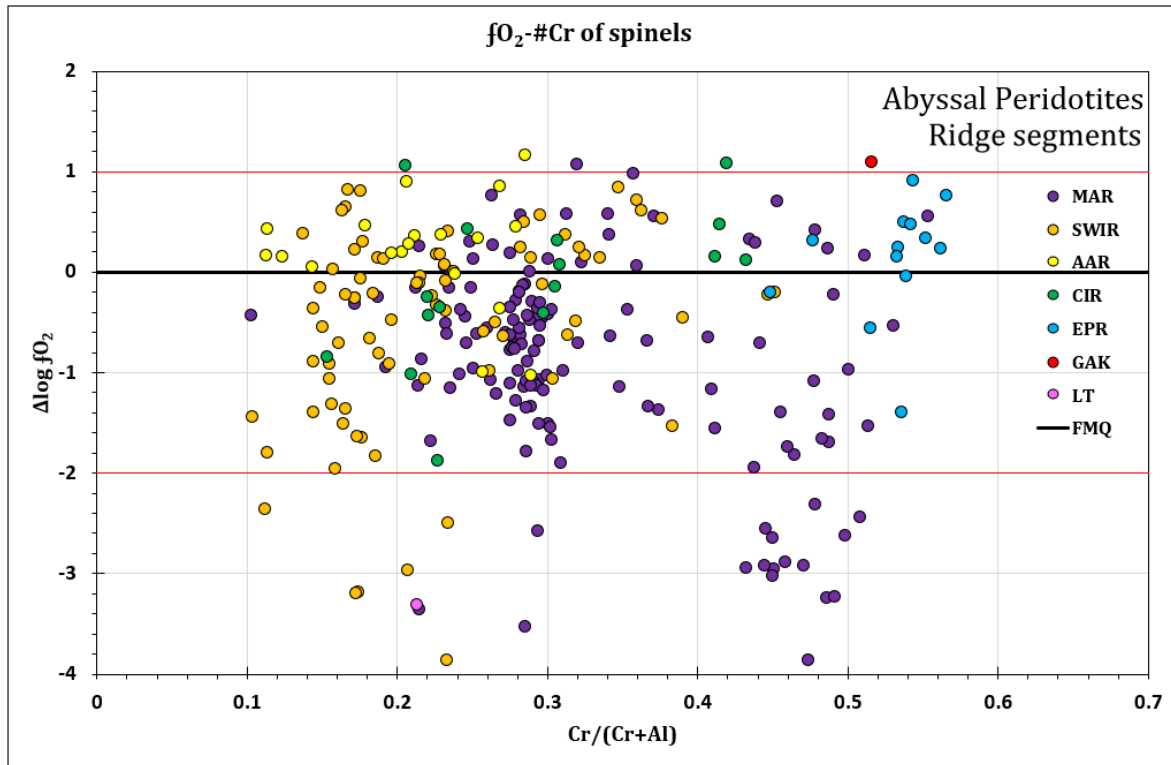


Figure 21: fO_2 given in log units relative to the FMQ equilibrium, plotted against the Cr# of spinels in the samples. The red lines indicate the range of fO_2 values that are representative of the upper mantle.

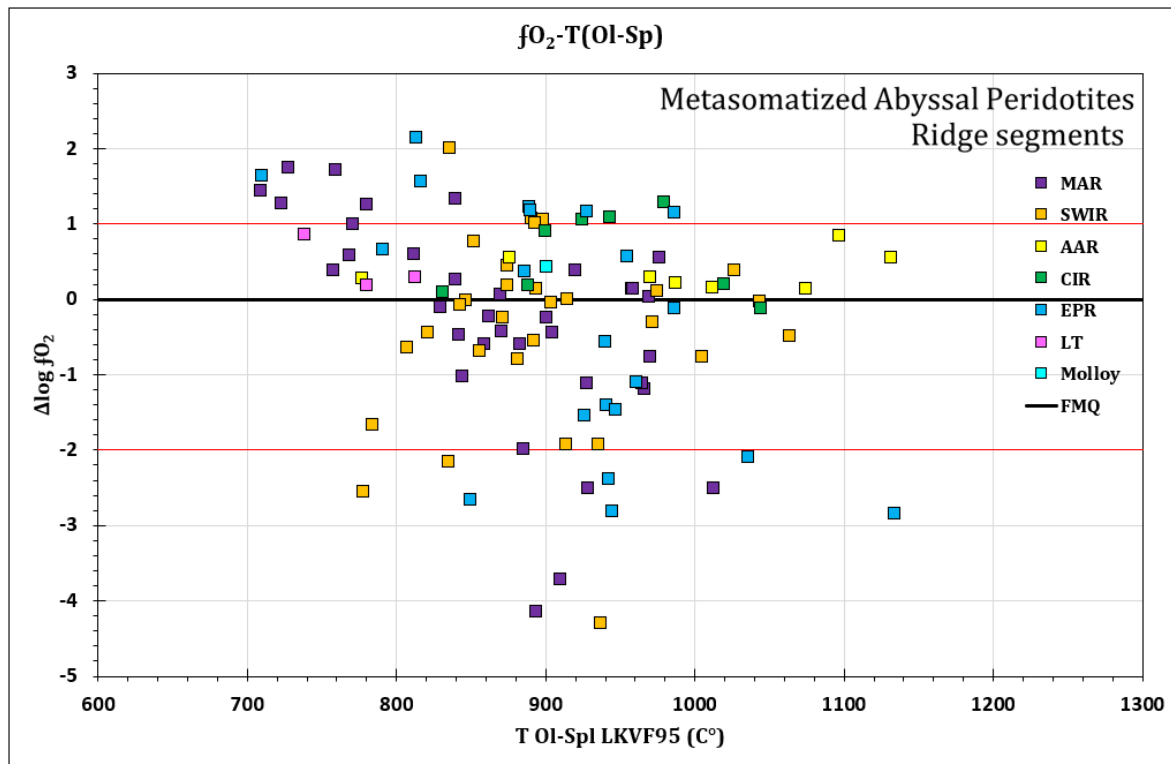


Figure 22: fO_2 given in log units relative to the FMQ equilibrium, plotted against T_{ol-spl} calculated with the LKVF95 geothermometer. The red lines indicate the range of fO_2 values that are representative of the upper mantle.

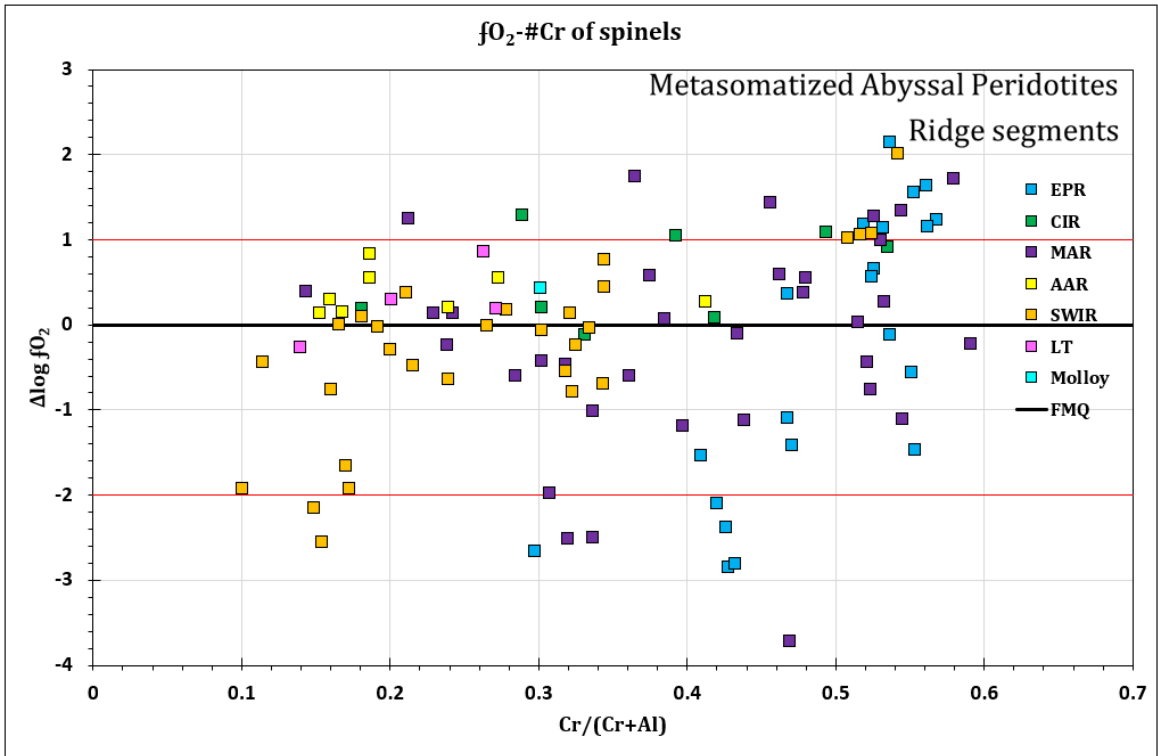


Figure 23: fO_2 given in log units relative to the FMQ equilibrium, plotted against the Cr# of spinels in the samples. The red lines indicate the range of fO_2 values that are representative of the upper mantle.

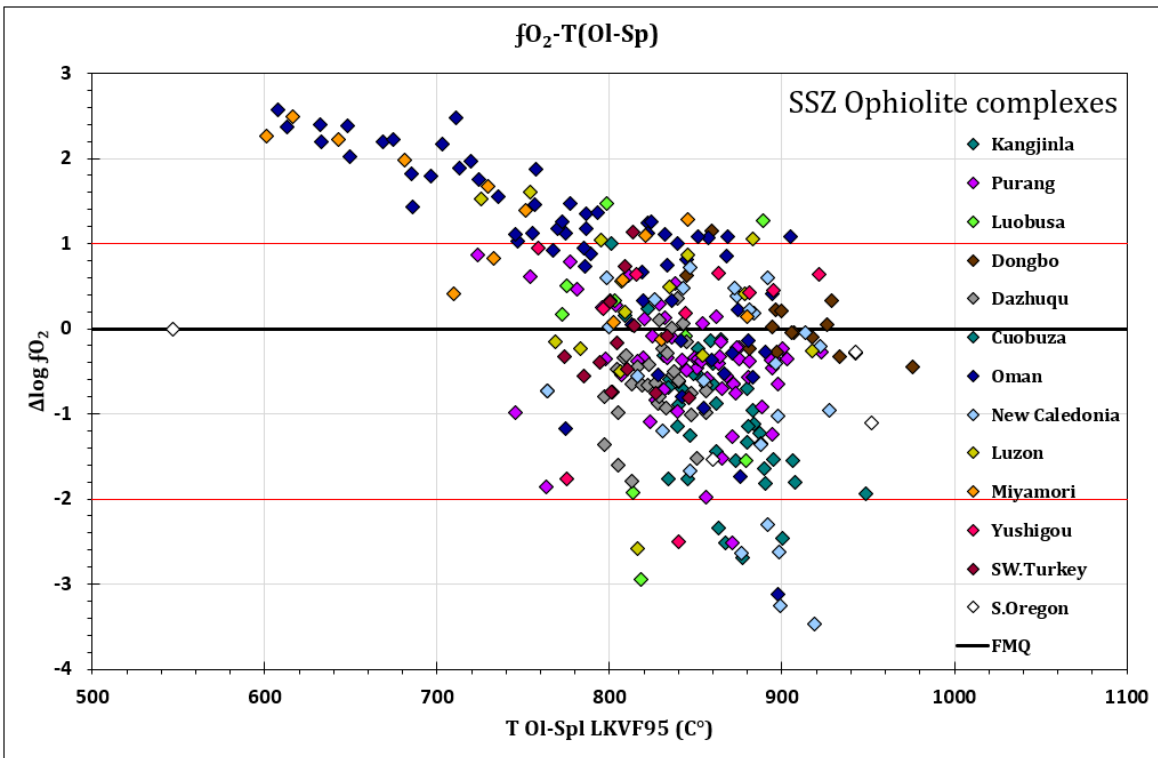


Figure 24: fO_2 given in log units relative to the FMQ equilibrium, plotted against T_{Ol-spl} calculated with the LKVF95 geothermometer. The red lines indicate the range of fO_2 values that are representative of the upper mantle.

which, combined with the high Cr# values might be taken to suggest metasomatism-induced melting. Regarding the temperatures of Fe-Mg exchange between olivine and spinel, T_{ol-spl} of the metasomatized abyssal peridotites range from 700°C to 1100°C. The samples that plot at lower temperatures (700°C–800°C) have probably undergone longer cooling times, shifting the Ol-Spl equilibrium to lower temperatures.

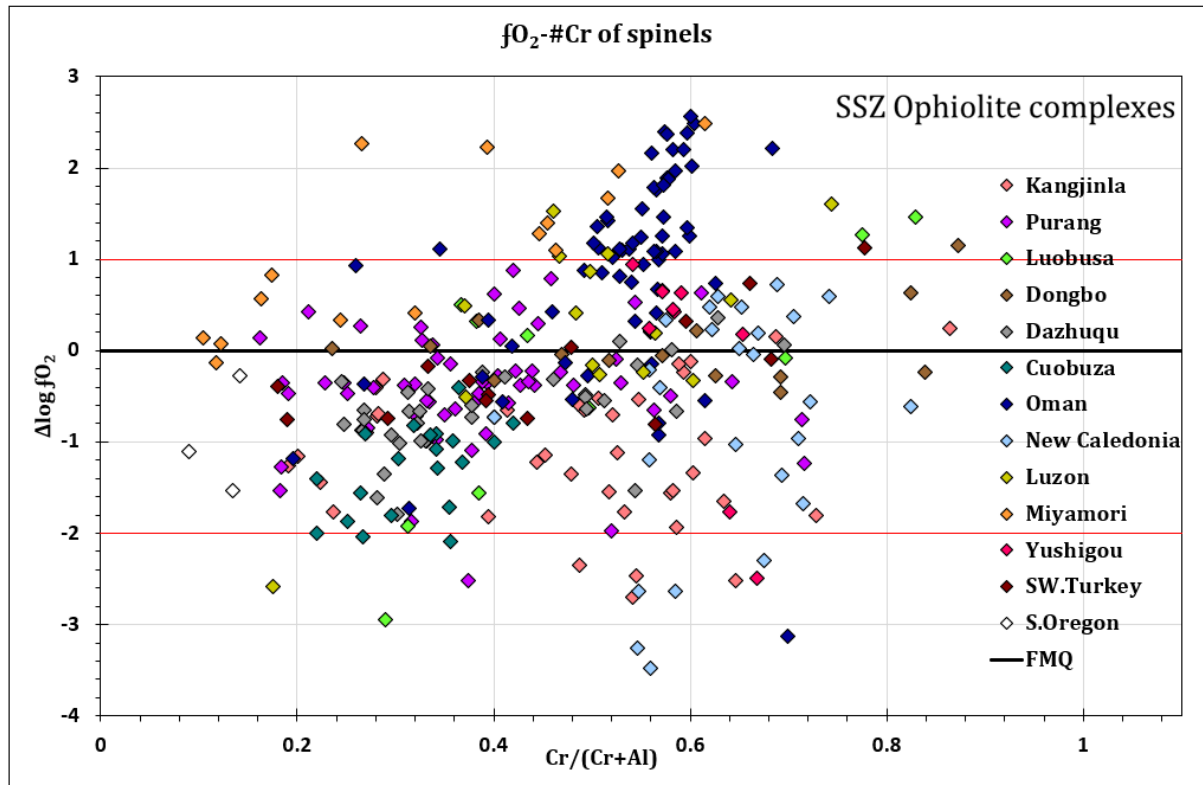
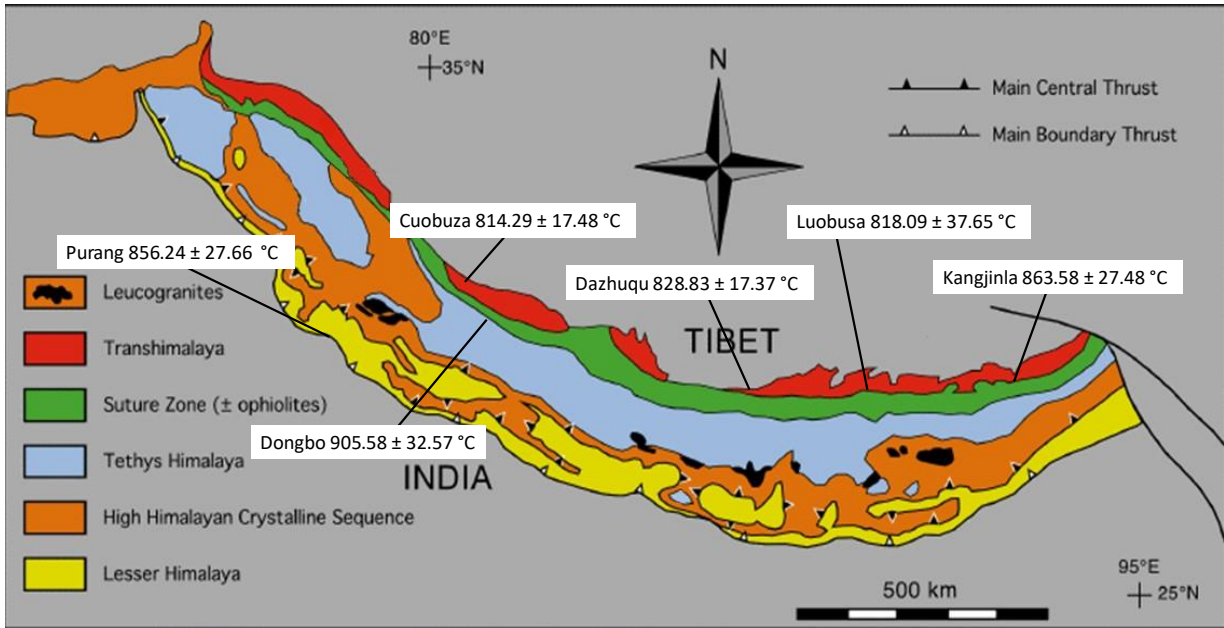


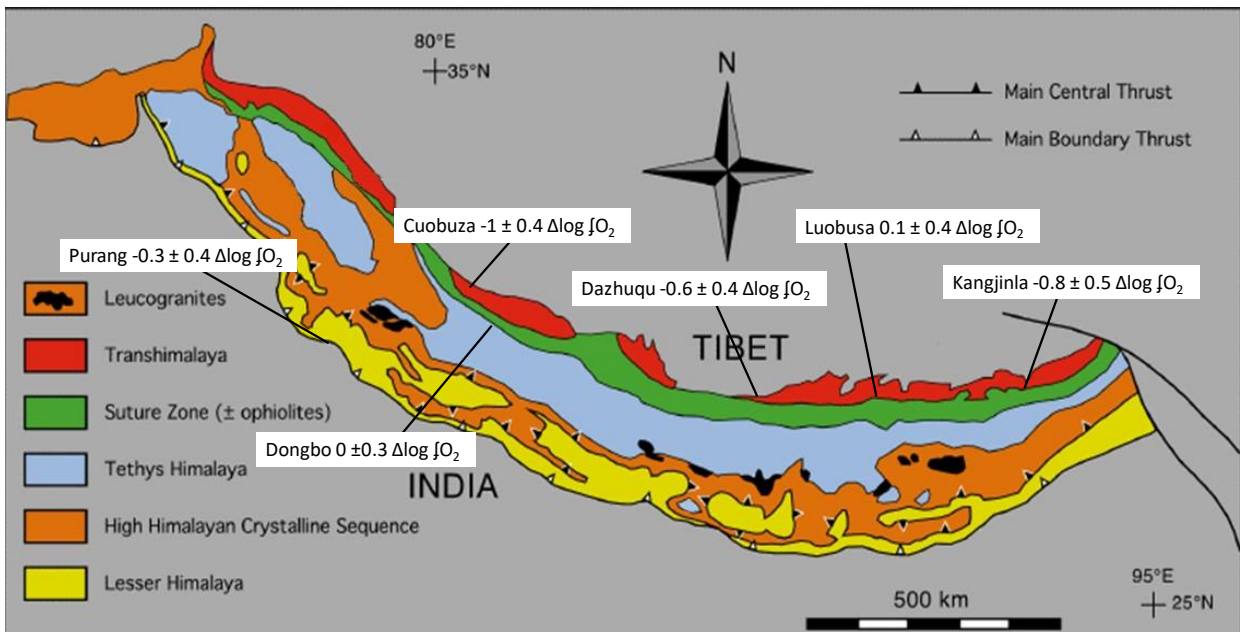
Figure 25: fO_2 given in log units relative to the FMQ equilibrium, plotted against the Cr# of spinels in the samples. The red lines indicate the range of fO_2 values that are representative of the upper mantle.

Figures 24 & 25 depict the redox state of ophiolitic peridotites in conjunction with their T_{ol-spl} and Cr#. In their majority, the samples indicate fO_2 values ranging from FMQ-2 to FMQ+1. The Cr# of the samples varies from 0.2 to 0.7, and T_{ol-spl} ranges from 600°C to 900°C. Samples from the Oman and the Miyamori complexes give the lowest equilibration temperatures indicating longer cooling times. These samples are also the ones with the higher values of fO_2 , plotting above FMQ+2, indicating a very oxidized environment, like the redox state of OIBs (Ballhaus, 1992). According to Fig. 25 most of the oxidized samples have high Cr# values. This is considered as the probable outcome of metasomatic processes that induce melting in an oxidizing environment.

Among the ophiolitic peridotites that were considered in this thesis, there are samples from complexes across the Yarlung-Tsangpo suture zone in Tibet. Pictures 5 & 6 show the spatial distribution of these bodies on a simplified regional geological map of the area with superimposed their calculated average fO_2 and T_{ol-spl} values.



Picture 5: Map of the Yarlung-Tsangpo suture zone showing the spatial distribution of ophiolitic bodies and their calculated average T_{ol-spl} values (LKVF95 thermometer).



Picture 6: Map of the Yarlung-Tsangpo suture zone showing the spatial distribution of ophiolitic bodies and their calculated average fO_2 values (Ballhaus et al., 1991 oxybarometer).

It can be seen that the most oxidized complex is the Luobusa complex ($0.1 \pm 0.4 \Delta \log fO_2$), whereas the most reduced complex is the Kangjinla complex ($-0.8 \pm 0.5 \Delta \log fO_2$). The Cuobuza complex displays the lowest average olivine-spinel equilibration temperatures ($814 \pm 17^\circ C$), suggesting a faster emplacement/exposure to the Earth's surface compared to the other complexes. The highest average temperature is calculated for the Dongbo complex ($906 \pm 33^\circ C$), indicating faster cooling rates in comparison with the other

complexes. Overall, the average oxygen fugacity of the suture zone is $-0.4 \pm 0.4 \Delta \log f_{O_2}$ and the average temperature of olivine-spinel equilibration is $848 \pm 35^\circ\text{C}$.

3.6 Redox state of peridotites in correlation with the $\text{Fe}^{3+}/\Sigma\text{Fe}$ ratio of spinels

The ratio $\text{Fe}^{3+}/\Sigma\text{Fe}$ represents the ratio of ferric to total iron (ferric plus ferrous) in spinel. It is a geochemical parameter that is used for the interpretation of the redox state of peridotites. The $\text{Fe}^{3+}/\Sigma\text{Fe}$ ratio in spinels can provide valuable information about the oxidation conditions prevailing during the formation of ultramafic rocks. To further examine the oxygen fugacity of the peridotites, the f_{O_2} values of each dataset were plotted against the $\text{Fe}^{3+}/\Sigma\text{Fe}$ ratios of their respective spinels.

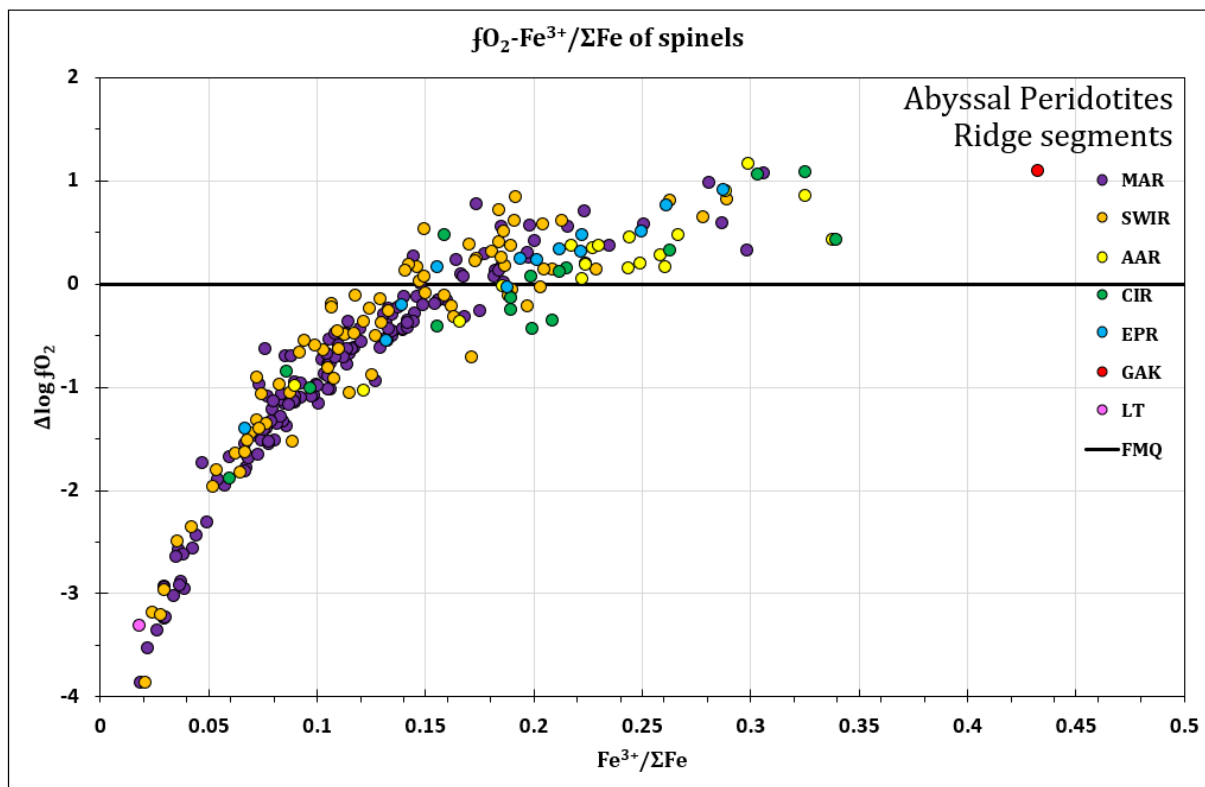


Figure 26: f_{O_2} given in log units relative to the FMQ equilibrium, plotted against the $\text{Fe}^{3+}/\Sigma\text{Fe}$ ratio of spinels in the samples.

As Fig. 26 shows, the $\text{Fe}^{3+}/\Sigma\text{Fe}$ ratios in non-metasomatized abyssal peridotites range from 0.025 to 0.35 while the oxygen fugacity of the same samples varies from FMQ-3 to FMQ+1. It is obvious that as the $\text{Fe}^{3+}/\Sigma\text{Fe}$ ratio of the samples increases the f_{O_2} values increase as well. Samples with higher $\text{Fe}^{3+}/\Sigma\text{Fe}$ values might indicate interaction with oxidizing fluids derived from seawater. On the other hand, the samples with lower $\text{Fe}^{3+}/\Sigma\text{Fe}$ and f_{O_2} values indicate a more reduced environment, appropriate of the suboceanic upper mantle.

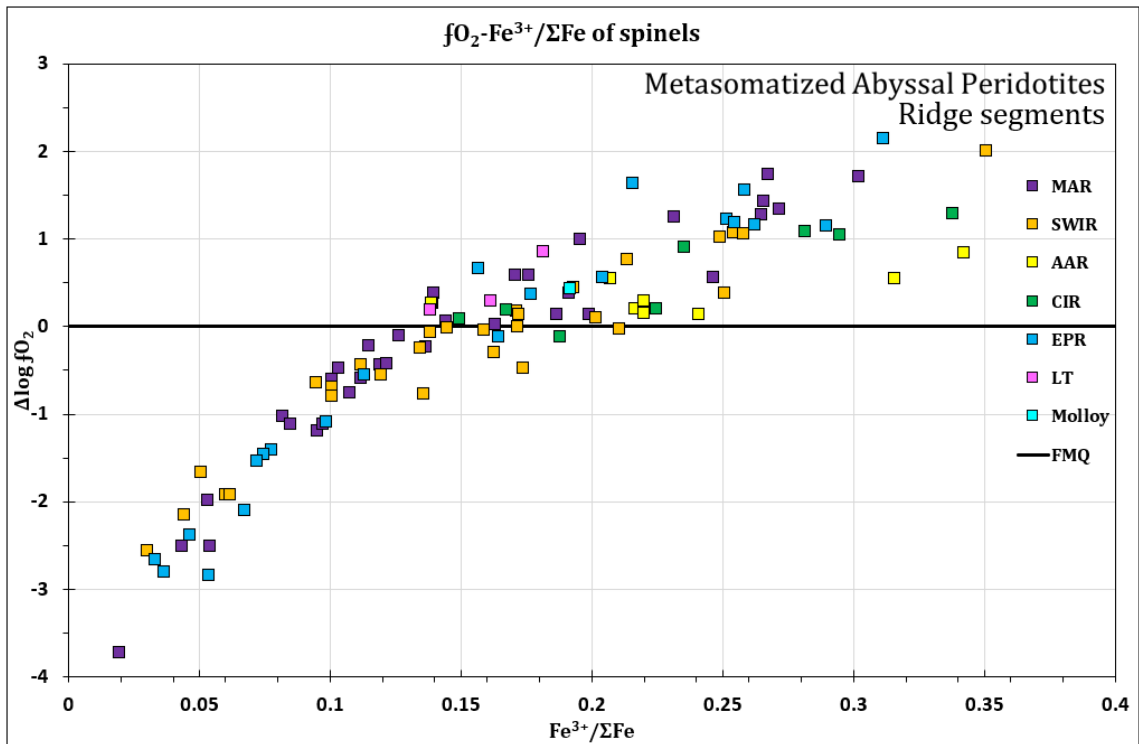


Figure 27: fO_2 given in log units relative to the FMQ equilibrium, plotted against the $Fe^{3+}/\Sigma Fe$ ratio of spinels in the samples.

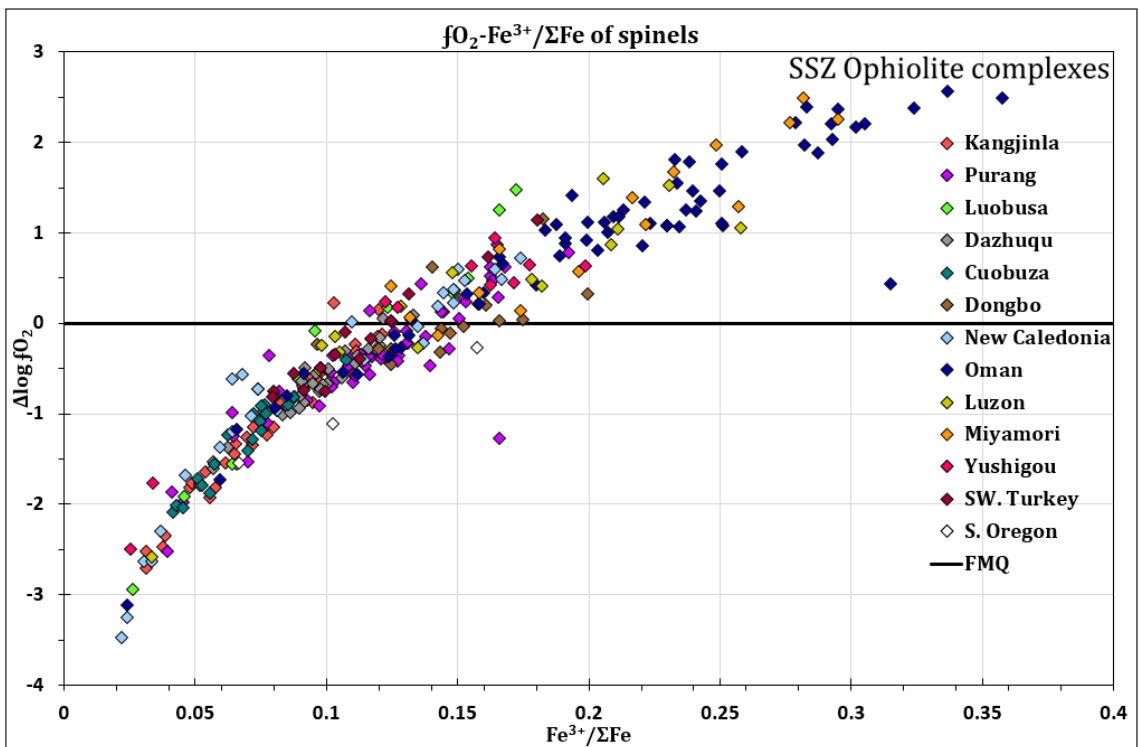


Figure 28: fO_2 given in log units relative to the FMQ equilibrium, plotted against the $Fe^{3+}/\Sigma Fe$ ratio of spinels in the samples.

Regarding the metasomatized abyssal peridotite samples, their spinel $Fe^{3+}/\Sigma Fe$ ratio varies from 0.05 to 0.35 likewise in the abyssal samples, whereas the fO_2 values range

from FMQ-3 to FMQ+2. (Fig. 27) Compared to the non-metasomatized abyssal peridotites the metasomatized samples are more oxidized in their majority indicating exposure to fluids and/or melts.

Ophiolitic peridotites are presented in Fig.28. Their $\text{Fe}^{3+}/\Sigma\text{Fe}$ values are similar to those of abyssal peridotites, ranging from 0.05 to 0.35, while their $f\text{O}_2$ values vary from FMQ-3 to above FMQ+2. Several samples plot below FMQ suggesting a more reduced environment. The more oxidized samples (Oman, Miyamori) may suggest interaction with fluids derived from the subducting slab, as subduction-related processes can, in general, lead to oxidizing conditions.

4. Summary and conclusions

In the present thesis the formation of the suboceanic upper mantle was explored via olivine-spinel equilibrium (temperatures of Fe-Mg exchange and oxygen fugacity conditions) across different geotectonic settings. Through a detailed examination of three distinct peridotite data sets (non-metasomatized abyssal peridotites, metasomatized abyssal peridotites, and ophiolitic SSZ peridotites), the thermal and redox state of the suboceanic upper mantle was assessed for these environments and possible processes affecting mantle evolution were discussed.

4.1 Results from peridotite spinel chemistry

Spinel in non-metasomatized abyssal peridotites are dominantly aluminum chromites, with higher Cr contents being associated with increased melting conditions, particularly in the fastest-spreading mid-ocean ridge, the East Pacific Rise (EPR). Spinel from metasomatized abyssal peridotites are also aluminum chromites in their majority, forming a trend toward chromian magnetite pointing to interactions with fluids. Spinel from ophiolitic mantle peridotites associated with subduction zones are predominantly chromian spinels signifying a more depleted mantle source. Samples from New Caledonia exhibit the highest depletion, while the Oman ophiolites suggest possible melt infiltration or metasomatic activity.

Compositional relationships between coexisting olivine and spinel provide additional information. Non-metasomatized abyssal peridotites display spinel Cr# – olivine Fo variations suggesting different degrees of mantle depletion, from peridotites indicating a fertile mantle source to peridotites associated with melt infiltration. Numerous metasomatized abyssal peridotites exhibit low Fo contents suggesting non-mantle-derived olivine, associated with melt crystallization. Ophiolitic SSZ peridotites (Fig.7) are the more depleted ones showing extensive partial melting. Plots of Al_2O_3 vs TiO_2 and Ti vs Cr# in spinel provide more insights into magma chemistry and tectonic provenance. Thus, non-metasomatized abyssal peridotites show mostly typical compositions, with some samples indicating MORB melt infiltration. Metasomatized abyssal samples point towards the OIB and MORB fields (Fig.9), indicating metasomatism from alkaline OIB and MORB melts respectively. SSZ ophiolites exhibit highly depleted compositions as their high Cr# suggests, while a part of the Oman ophiolite points toward the OIB field implying OIB melt infiltration.

4.2 Results from olivine-spinel equilibration temperatures and oxygen fugacities

To investigate the redox state and the thermal conditions of the suboceanic upper mantle in major ocean basins and supra-subduction zone environments a comprehensive analysis of geothermometry and oxybarometry was undertaken. This discussion combines findings from the examination of Fe-Mg exchange temperatures between olivine and spinel calculated with the LKVF95 geothermometer, the values of oxygen fugacity (fO_2) calculated with the oxybarometer calibrated by Ballhaus et al., 1991, and Cr#- fO_2 and fO_2 - $Fe^{3+}/\Sigma Fe$ variations in spinels.

Temperature Analysis

The temperatures obtained from the LKVF95 thermometer reveal significant differences across settings. Non-metasomatized abyssal peridotites display equilibration temperatures ranging between 800°C and 1000°C with a minority reaching above 1000°C. These higher temperatures suggest rapid emplacement that blocked Fe-Mg diffusion early during cooling. By contrast, the metasomatized abyssal samples illustrate a broader temperature range (700°C to 1100°C) with lower temperatures (700°C-800°C) indicating prolonged cooling. Ophiolitic SSZ peridotites exhibit the lowest temperatures varying from 600°C to 900°C, indicating extended cooling periods.

Redox State Assessment

The redox state, a crucial factor in understanding mantle processes and mineral stability, varies across geotectonic settings. The fO_2 values, plotted against spinel Cr# and $Fe^{3+}/\Sigma Fe$, offer a detailed view of the oxidizing conditions. Non-metasomatized abyssal peridotites indicate a more reducing environment, with fO_2 values ranging from FMQ-2 to FMQ. The presence of samples with higher $Fe^{3+}/\Sigma Fe$ ratios and corresponding fO_2 values indicates interaction with hydrothermal fluids. Metasomatized abyssal samples present a wider range of fO_2 values with significant evidence of oxidation at conditions between FMQ+1 and FMQ+2. This is most likely the outcome of metasomatic processes where fluid-rocks interactions introduce more oxidizing conditions. The ophiolitic SSZ peridotites, exhibit the highest fO_2 values among settings ranging from FMQ-2 to above FMQ+2. While many samples indicate a reduced environment, there is a noticeable subset with values plotting above FMQ+2 suggesting severe oxidation, as is particularly evident in samples from Oman. The lower equilibration temperatures and the presence of high Cr# in more oxidized samples stress the role of metasomatism, probably linked to fluids derived from the subducting slab.

The comparison across settings underlines the impact of geological environment on mantle temperature and redox. While abyssal peridotites represent a relatively homogenous and reduced mantle source, metasomatized and SSZ peridotites reflect complex interactions between mantle rocks and metasomatic processes, leading to more

oxidizing conditions. This underscores the importance of considering both geothermometric and oxybarometric data in reconstructing the thermal and chemical evolution of the suboceanic upper mantle.

References

- Arai, S. (1994). Characterization of spinel peridotites by olivine-spinel compositional relationships: Review and interpretation. *Chemical Geology*, 113(3-4), pp.191–204. doi: [https://doi.org/10.1016/0009-2541\(94\)90066-3](https://doi.org/10.1016/0009-2541(94)90066-3).
- Ballhaus, C. (1993). Redox states of the lithospheric and asthenospheric upper mantle. *Contributions to Mineralogy and Petrology*, 114(3), pp.331–348. doi: <https://doi.org/10.1007/bf01046536>.
- Ballhaus, C., Berry, R.F. and Green, D.H. (1994). High-pressure experimental calibration of the olivine-orthopyroxene-spinel oxygen geobarometer: implications for the oxidation state of the upper mantle. *Contributions to Mineralogy and Petrology*, 118(1), pp.109–109. doi: <https://doi.org/10.1007/bf00310615>.
- BARNES, S.J. and ROEDER, P.L. (2001). The Range of Spinel Compositions in Terrestrial Mafic and Ultramafic Rocks. *Journal of Petrology*, 42(12), pp.2279–2302. doi: <https://doi.org/10.1093/petrology/42.12.2279>.
- Birner, S.K., Cottrell, E., Warren, J.M., Kelley, K.A. and Davis, F.A. (2018). Peridotites and basalts reveal broad congruence between two independent records of mantle fO₂ despite local redox heterogeneity. *Earth and Planetary Science Letters*, 494, pp.172–189. doi: <https://doi.org/10.1016/j.epsl.2018.04.035>.
- Birner, S.K., Cottrell, E., Warren, J.M., Kelley, K.A. and Davis, F.A. (2021). Melt addition to mid-ocean ridge peridotites increases spinel Cr# with no significant effect on recorded oxygen fugacity. *Earth and Planetary Science Letters*, 566, p.116951. doi: <https://doi.org/10.1016/j.epsl.2021.116951>.
- Birner, S.K., Warren, J.M., Cottrell, E. and Davis, F.A. (2016). Hydrothermal alteration of seafloor peridotites does not influence oxygen fugacity recorded by spinel oxybarometry. *Geology*, 44(7), pp.535–538. doi: <https://doi.org/10.1130/g38113.1>.
- Birner, S.K., Warren, J.M., Cottrell, E., Davis, F.A., Kelley, K.A. and Falloon, T.J. (2017). Forearc Peridotites from Tonga Record Heterogeneous Oxidation of the Mantle following Subduction Initiation. *Journal of Petrology*, 58(9), pp.1755–1780. doi: <https://doi.org/10.1093/petrology/egx072>.
- Bonatti, E. and Michael, P.J. (1989). Mantle peridotites from continental rifts to ocean basins to subduction zones. *Earth and Planetary Science Letters*, 91(3-4), pp.297–311. doi: [https://doi.org/10.1016/0012-821x\(89\)90005-8](https://doi.org/10.1016/0012-821x(89)90005-8).
- Bosi, F., Biagioni, C. and Pasero, M. (2019). Nomenclature and classification of the spinel supergroup. *European Journal of Mineralogy*, 31(1), pp.183–192. doi: <https://doi.org/10.1127/ejm/2019/0031-2788>.
- Bryndzia, L.T. and Wood, B.J. (1990). Oxygen thermobarometry of abyssal spinel peridotites; the redox state and C-O-H volatile composition of the Earth's sub-oceanic upper mantle. *American Journal of Science*, 290(10), pp.1093–1116. doi: <https://doi.org/10.2475/ajs.290.10.1093>.

Cannaò, E. and Malaspina, N. (2018). From oceanic to continental subduction: Implications for the geochemical and redox evolution of the supra-subduction mantle. *Geosphere*, 14(6), pp.2311–2336. doi: <https://doi.org/10.1130/ges01597.1>.

Caran, Ş., Çoban, H., Flower, M.F.J., Ottley, C.J. and Yılmaz, K. (2010). Podiform chromitites and mantle peridotites of the Antalya ophiolite, Isparta Angle (SW Turkey): Implications for partial melting and melt–rock interaction in oceanic and subduction-related settings. *Lithos*, 114(3-4), pp.307–326. doi: <https://doi.org/10.1016/j.lithos.2009.09.006>.

Chen, Y.D., Pearson, N.J., O'Reilly, S.Y. and Griffin, W.L. (1991). Applications of Olivine-Orthopyroxene-Spinel Oxygen Geobarometers to the Redox State of the Upper Mantle. *Journal of Petrology*, Special Volume (2), pp.291–306. doi: https://doi.org/10.1093/petrology/special_volume.2.291.

Davis, F.A. and Cottrell, E. (2018). Experimental investigation of basalt and peridotite oxybarometers: Implications for spinel thermodynamic models and Fe³⁺ compatibility during generation of upper mantle melts. *American Mineralogist*, 103(7), pp.1056–1067. doi: <https://doi.org/10.2138/am-2018-6280>.

Davis, F.A., Cottrell, E., Birner, S.K., Warren, J.M. and Lopez, O.G. (2017). Revisiting the electron microprobe method of spinel-olivine-orthopyroxene oxybarometry applied to spinel peridotites. *American Mineralogist*, 102(2), pp.421–435. doi: <https://doi.org/10.2138/am-2017-5823>.

Dick, H.J.B. and Bullen, T. (1984). Chromian spinel as a petrogenetic indicator in abyssal and alpine-type peridotites and spatially associated lavas. *Contributions to Mineralogy and Petrology*, 86(1), pp.54–76. doi: <https://doi.org/10.1007/bf00373711>.

Dick, H.J.B., Fisher, R.L. and Bryan, W.B. (1984). Mineralogic variability of the uppermost mantle along mid-ocean ridges. *Earth and Planetary Science Letters*, 69(1), pp.88–106. doi: [https://doi.org/10.1016/0012-821x\(84\)90076-1](https://doi.org/10.1016/0012-821x(84)90076-1).

Evans, B.W. and Frost, B. Ronald. (1975). Chrome-spinel in progressive metamorphism—a preliminary analysis. *Geochimica et Cosmochimica Acta*, 39(6-7), pp.959–972. doi: [https://doi.org/10.1016/0016-7037\(75\)90041-1](https://doi.org/10.1016/0016-7037(75)90041-1).

Evans, K.A., Reddy, S.M., Tomkins, A.G., Crossley, R.J. and Frost, B.R. (2017). Effects of geodynamic setting on the redox state of fluids released by subducted mantle lithosphere. *Lithos*, 278-281, pp.26–42. doi: <https://doi.org/10.1016/j.lithos.2016.12.023>.

Fabriés, J. (1979). Spinel-Olivine Geothermometry in Peridotites from Ultramafic Complexes. *Contrib. Mineral. Petrol*, 69, pp.329–336.

Feng, G., Yang, J., Niu, X., Liu, F., Qiu, T. and Dilek, Y. (2021). Formation processes and tectonic implications of mantle peridotites of the Yushigou ophiolite in the North Qilian Orogenic Belt, NW China. *Lithos*, 400-401, p.106430. doi: <https://doi.org/10.1016/j.lithos.2021.106430>.

- Ferracutti, G.R., Gargiulo, M.F., Ganuza, M.L., Bjerg, E.A. and Castro, S.M. (2014). Determination of the spinel group end-members based on electron microprobe analyses. *Mineralogy and Petrology*, 109(2), pp.153–160. doi: <https://doi.org/10.1007/s00710-014-0363-1>.
- Foley, S.F. (2010). A Reappraisal of Redox Melting in the Earth's Mantle as a Function of Tectonic Setting and Time. *JOURNAL OF PETROLOGY*, 52(7-8), pp.1363–1391. doi: <https://doi.org/10.1093/petrology/egq061>.
- Frisch, W., Meschede, M. and Blakey, R.C. (2011). *Plate Tectonics*. Berlin, Heidelberg: Springer Berlin Heidelberg. doi: <https://doi.org/10.1007/978-3-540-76504-2>.
- Frost, D.J. and McCammon, C.A. (2008). The Redox State of Earth's Mantle. *Annual Review of Earth and Planetary Sciences*, 36(1), pp.389–420. doi: <https://doi.org/10.1146/annurev.earth.36.031207.124322>.
- Gamal El Dien, H., Arai, S., Doucet, L.-S., Li, Z.-X., Kil, Y., Fougereuse, D., Reddy, S.M., Saxey, D.W. and Hamdy, M. (2019). Cr-spinel records metasomatism not petrogenesis of mantle rocks. *Nature Communications*, 10(1). doi: <https://doi.org/10.1038/s41467-019-13117-1>.
- Greenfield, A.M.R., Ghent, E.D. and Russell, J.K. (2013). Geothermobarometry of spinel peridotites from southern British Columbia: implications for the thermal conditions in the upper mantle. *Canadian Journal of Earth Sciences*, 50(10), pp.1019–1032. doi: <https://doi.org/10.1139/cjes-2013-0037>.
- Hellebrand, E., Snow, J.E., Dick, H.J.B. and Hofmann, A.W. (2001). *Coupled major and trace elements as indicators of the extent of melting in mid-ocean-ridge peridotites*, *NATURE*, VOL 410, p.677-681. www.nature.com.
- HERZBERG, C. (2004). Geodynamic Information in Peridotite Petrology. *Journal of Petrology*, 45(12), pp.2507–2530. doi: <https://doi.org/10.1093/petrology/egh039>.
- Hu, W., Zhou, M., Ribeiro, J.M., Malpas, J., Wu, Y. and Bai, Z. (2023). The Redox State of Incipient Oceanic Subduction Zones: An Example from the Troodos Ophiolite (Cyprus). *Journal of Geophysical Research: Solid Earth*, 128(4). doi: <https://doi.org/10.1029/2022jb025008>.
- Jianping, L., Kornprobst, J., Vielzeuf, D. and Fabriés, J. (1995). An improved experimental calibration of the olivine-spinel geothermometer. *Chinese Journal of Geochemistry*, 14(1), pp.68–77. doi: <https://doi.org/10.1007/bf02840385>.
- Kamenetsky, V., Crawford, A. and Meffre, S. (2001). Maurel & Maurel, 1982a, subaerial lavas and peridotites. Unlike mg-number, Cr-spinel Al₂O₃ 1982b; Sack. *JOURNAL OF PETROLOGY*, 42(2), pp.655–671.
- KAMENETSKY, V.S. (2001). Factors Controlling Chemistry of Magmatic Spinel: An Empirical Study of Associated Olivine, Cr-spinel and Melt Inclusions from Primitive Rocks. *Journal of Petrology*, 42(4), pp.655–671. doi: <https://doi.org/10.1093/petrology/42.4.655>.

Kuwahara, H. and Nakada, R. (2023). Partitioning of Fe²⁺ and Fe³⁺ between bridgmanite and silicate melt Implications for redox evolution of the Earth's mantle. *Earth and Planetary Science Letters*, 615, p.118197. doi <https://doi.org/10.1016/j.epsl.2023.118197>.

Lee, C.-T.A., Luffi, P., Le Roux, V., Dasgupta, R., Albarède, F. and Leeman, W.P. (2010). The redox state of arc mantle using Zn/Fe systematics. *Nature*, 468(7324), pp.681–685. doi: <https://doi.org/10.1038/nature09617>.

Li, J., Kornprobst, J., Vielzeuf, D. and Fabriés, J. (1995). An Improved Experimental Calibration of the Olivine-Spinel Geothermometer of. *CHINESE JOURNAL OF GEOCHEMISTRY*, 14(1).

Michael, P.J. and Bonatti, E. (1985). Peridotite composition from the North Atlantic: regional and tectonic variations and implications for partial melting. *Earth and Planetary Science Letters*, 73(1), pp.91–104. doi: [https://doi.org/10.1016/0012-821x\(85\)90037-8](https://doi.org/10.1016/0012-821x(85)90037-8).

Neil C., M. (2017). *Submarine Geomorphology*. [online] pp.349–365. Available at: <https://link.springer.com/book/10.1007/978-3-319-57852-1>.

Nikolaev, G.S., Ariskin, A.A., Barmina, G.S., Nazarov, M.A. and Almeev, R.R. (2016). Test of the Ballhaus–Berry–Green Ol–Opx–Sp oxybarometer and calibration of a new equation for estimating the redox state of melts saturated with olivine and spinel. *Geochemistry International*, 54(4), pp.301–320. doi <https://doi.org/10.1134/s0016702916040078>.

Norikatsu Akizawa, Arai, S. and Tamura, A. (2012). Behavior of MORB magmas at uppermost mantle beneath a fast-spreading axis: an example from Wadi Fizh of the northern Oman ophiolite. *Contributions to Mineralogy and Petrology*, 164(4), pp.601–625. doi: <https://doi.org/10.1007/s00410-012-0762-4>.

OHARA, Y. and ISHII, T. (1998). Peridotites from the southern Mariana forearc: Heterogeneous fluid supply in mantle wedge. *The Island Arc*, 7(3), pp.541–558. doi: <https://doi.org/10.1111/j.1440-1738.1998.00209.x>.

Ozawa, K. (1988). Ultramafic tectonite of the Miyamori ophiolitic complex in the Kitakami Mountains, Northeast Japan: hydrous upper mantle in an island arc. *Contributions to Mineralogy and Petrology*, 99(2), pp.159–175. doi: <https://doi.org/10.1007/bf00371458>.

Réjean Hébert, Khalid Gueddari, M.R. Laflèche, Marie-Odile Beslier and Véronique Gardien (2001). Petrology and Geochemistry of Exhumed Peridotites and gabbros at non-volcanic margins: ODP Leg 173 West Iberia ocean-continent transition zone. *Geological Society, London, Special Publications*, 187(1), pp.161–189. doi <https://doi.org/10.1144/gsl.sp.2001.187.01.09>.

Rohrbach, A., Ballhaus, C., Ulmer, P., Golla-Schindler, U. and Schönbohm, D. (2011). Experimental Evidence for a Reduced Metal-saturated Upper Mantle. *Journal of Petrology*, 52(4), pp.717–731. doi: <https://doi.org/10.1093/petrology/egq101>.

Searle, M.P. and Cox, J. (1999). Tectonic setting, origin, and obduction of the Oman ophiolite. *Geological Society of American Bulletin*, pp.104–112. doi: [https://doi.org/10.1130/0016-7606\(1999\)111%3C0104:TSOAO0%3E2.3.CO;2](https://doi.org/10.1130/0016-7606(1999)111%3C0104:TSOAO0%3E2.3.CO;2).

Skolotnev, S.G., Dobrolyubova, K.O., Peyve, A.A., S. Yu. Sokolov, Чамов, H.П. and Ligi, M. (2022). Structure of Spreading Segments of the Mid-Atlantic Ridge between the Arkhangelsky and Bogdanov Transform Faults, Equatorial Atlantic. *Geotectonics*, 56(1), pp.1–20. doi <https://doi.org/10.1134/s0016852122010083>.

Song, S., Su, L., Niu, Y., Lai, Y. and Zhang, L. (2009). CH₄ inclusions in orogenic harzburgite: Evidence for reduced slab fluids and implication for redox melting in mantle wedge. *Geochimica et Cosmochimica Acta*, 73(6), pp.1737–1754. doi: <https://doi.org/10.1016/j.gca.2008.12.008>.

Srrvnns, R., Suraey, U. and Ngton, D', W. (1944). COMPOSITION OF SOME CHROMITES OF THE WESTERN HEMISPHERE. *THE AMERICAN MINERALOGIST JOURNAL OF THE MINERALOGICAL SOCIETY OF AMERICA*, 29.

Stracke, A. (2015). Depleted Mantle. *Springer eBooks*, pp.1–5. doi https://doi.org/10.1007/978-94-007-6644-0_11-4.

Warren, J.M. (2016). Global variations in abyssal peridotite compositions. *Lithos*, pp.193–219.

Warren, J.M., Shimizu, N., Sakaguchi, C., Dick, H.J.B. and Nakamura, E. (2009). An assessment of upper mantle heterogeneity based on abyssal peridotite isotopic compositions. *Journal of Geophysical Research: Solid Earth*, 114(B12). doi <https://doi.org/10.1029/2008jb006186>.

Wood', B. (1990). AN EXPERIMENTAL TEST OF THE SPINEL PERIDOTITE OXYGEN BAROMETER. *JOURNAL OF GEOPHYSICAL RESEARCH*, 95(B10), pp.845–860.

Workman, R.K. and Hart, S.R. (2005). Major and trace element composition of the depleted MORB mantle (DMM). *Earth and Planetary Science Letters*, 231(1-2), pp.53–72. doi: <https://doi.org/10.1016/j.epsl.2004.12.005>.

Xu, Y., Liu, C. and Lin, W. (2000). Melt extraction and reaction in the forearc mantle: Constraints from trace elements and isotope geochemistry of ultra-refractory peridotites of the New Caledonia Peridotite Nappe. *Lithos*, 380-381, pp.1–19.

Zhang, H.L., Hirschmann, M.M., Cottrell, E. and Withers, A.C. (2017). Effect of pressure on Fe³⁺/ΣFe ratio in a mafic magma and consequences for magma ocean redox gradients. *Geochimica et Cosmochimica Acta*, 204, pp.83–103. doi: <https://doi.org/10.1016/j.gca.2017.01.023>.